Doctoral Dissertation

Studies on Low-voltage Dual-gate Organic Transistor based Pressure-sensing Devices

OGUNLEYE, Olamikunle Osinimu

Supervisor: Professor Hideyuki Murata

Graduate School of Advanced Science and Technology

Japan Advanced Institute of Science and Technology

Materials Science

December 2019

Studies on Low-voltage Dual-gate Organic Transistor based Pressure-sensing Devices

OGUNLEYE, Olamikunle Osinimu

1620402

Pressure sensing devices are essential for monitoring daily activities, health conditions, and environmental pressure. These devices make use of transistors to amplify signals from the sensing elements. However, the sensors commercially available today are mostly made up of inorganic materials of which the drawback of these materials are: they are rigid, require high temperatures, and expensive to manufacture.

Research into organic materials has made it possible to fabricate pressure-sensing devices using organic materials for sensors as well as read-out elements (transistors). However, the high power consumption of these pressure sensors hinders the commercial viability of these sensors. The reason for the high power consumption is due to the high operation voltage (usually greater than 10 V) of organic transistors used in these devices.

Recently, our laboratory developed a low-voltage dual-gate organic transistor pressure sensing device using P(VDF-TrFE) as the sensor and an OFET with operation voltage of -5 Vfor signal amplification.

This dissertation focuses on investigating the sensing mechanism of the pressure sensing device by quantitative analysis. Firstly, developing a low-voltage OFET using a novel biopolyamide as the dielectric. The device showed p-type transfer and output characteristics. In addition, using crosslinked poly (vinyl cinnamate) as the dielectric, a low-voltage OFET was equally fabricated and characterized.

Secondly, a dual-gate pressure sensor, using the low-voltage OFET as read-out element and P(VDF-TrFE) as the sensing element was fabricated and characterized. The device showed a linear relationship between the magnitude of pressure exerted on the sensor, and the threshold voltage shift displayed.

Thirdly, in order to understand the sensing mechanism of the pressure sensor, the quantity of charges generated by the piezoelectric film was estimated by developing a low-voltage dual-gate OFET using CYTOP as the top-gate dielectric. The threshold voltage could be linearly controlled by the top-gate voltage with results similar to the pressure sensing device.

Using this information, d_{33} of the piezoelectric film was quantified to be 72 pC/N. This was confirmed directly using a piezoelectric measurement system to be 53 pC/N. Based on these results, I was able to conclude that the operation of this device was due to the piezoelectric nature of the P(VDF-TrFE) film.

In the latter part of the dissertation, the investigation of the magnitude of the electric field strength with respect to the initial threshold shift caused by the piezoelectric layer was carried out. Results obtained showed that increasing the electric field strength gave rise to an increase in the threshold shift.

This research is promising because the sensing voltage from the polarized P(VDF-TrFE) provides an adequate signal which can be amplified by a low-voltage OFET. This configuration of pressure sensors is promising for future wearable devices because of the low power consumption involved.

Keywords: P(VDF-TrFE), Dual-gate OFET; threshold voltage; piezoelectric constant (d_{33}), dual-gate organic pressure sensor.

Acknowledgment

I would like to thank my supervisor Professor Hideyuki Murata of the school of materials science, Japan Advanced Institute of Science and Technology (JAIST) for the opportunity to be a research student, then a doctoral student in his laboratory. I also wish to thank him for his excellent supervision and support throughout the program. Also, I want to thank Associate Professor Heisuke Sakai for his intellectual support, suggestions, and contributions to my research.

I sincerely appreciate the examination committee members, Professor Eisuke Tokumitsu, Professor Susumu Horita, and Associate Professor Yuki Nagao. I also wish to deeply appreciate Professor Kenji Ishida, Kobe University for his evaluation and assessment of this research work.

I want to thank Yoshinaka-san, Professor Kaneko, and Associate Professor Yuya Ishii for their contributions towards this research.

I am grateful to the Embassy of Japan, Nigeria for selecting me for the prestigious Ministry of Education, Culture, Sports, Science, and Technology (MEXT) scholarship and the ministry for giving me the necessary financial support during my stay and studies in Japan.

My sincere gratitude goes to my fiancée for standing by me despite the distance; my parents and my sister for their overwhelming psychological support during my studies.

Content

List of symbols

Symbols	Meaning
A	Area of capacitor plates
C	Capacitance
d	Thickness of the insulator in a capacitor
e	Elementary charge
I_G	Gate current
I_D	Drain current
k	Dielectric constant
mV/dec	millivolts/decade
V	Voltage
V_D	Drain voltage
V_G	Gate voltage
V_{th}	Threshold voltage
SS	Subthreshold swing
W	Channel width
ε	Permittivity of the material
μ	Saturation field-effect mobility

List of Abbreviations

Abbreviations	Meanings
AFM	Atomic force microscopy
CYTOP	poly(perflurobutenylvinylether)
HMDS	Hexamethyldisilazane
IPA	Isopropyl alcohol
ITO	Indium tin oxide
MIM	Metal/Insulator/Metal
OFET	Organic field-effect transistor
PDMS	Polydimethylsiloxane
PEN	Polyethylene naphthalate
PET	Polyethylene terephthalate
PVCN	Poly(vinyl cinnamate)
P(VDF-TrFE)	Poly(vinylidene fluoride-trifluoroethylene)
TIPS-pentacene	6,13-Bis(triisopropylsilylehthynyl)pentacene

CHAPTER 1 || INTRODUCTION

1.1. Organic Devices

Printed electronic sensors with low-cost and low-power consumption have to be developed to create a smarter and more efficient ecosystem than the one we have today. This system could boost safety and living standards. The current goal is to drive societies based on the internet of things and big data storage [1-3]. To create societies based on these technologies, trillions of sensors have to be easily manufactured and disposed of when damaged or old without causing harm to the environment [4]. Increasing the volume of sensors depends mainly on the materials used to produce them. Unlike silicon-based devices, organic devices require low-cost, facile solution processing conditions, at low temperatures (<= 100 ^{o}C) in large areas [5, 6]. Employing solution processing methods, organic materials are deposited on various types of substrates, which includes flexible substrates such as PET and PEN, therefore making it possible to manufacture flexible devices [7, 8]. These devices include organic field-effect transistors (OFETs), organic light emitting diodes (OLED), and organic solar cells [9-11]. OFETs have been used to amplify signals from sensing signals such as pressure and temperature by utilizing them in connection with sensors which can detect pressure, temperature signals [12, 13]. These sensors could be applied for health care monitoring by the diagnosis of vital signs such as blood pressure and body temperature [14].

In this chapter, various types of pressure sensing elements will be introduced as well as OFET based pressure sensing devices. In addition, the current issues facing the commercialization of th this type of pressure sensors would be discussed as well as previous research done by former students in OFET group will also be discussed.

1.2. General Introduction to pressure-sensing devices.

Pressure sensors may be classified majorly into the pressure ranges (<10 kPa, 10-100 kPa, >100 kPa) in which they operate and their transduction mechanism [15]. This section gives a literature survey of both in section 1.2.1 and 1.2.2.

1.2.1. Pressure regimes

Pressure regimes of pressure sensors could be classified majorly into three categories as seen in Figure 1.1.

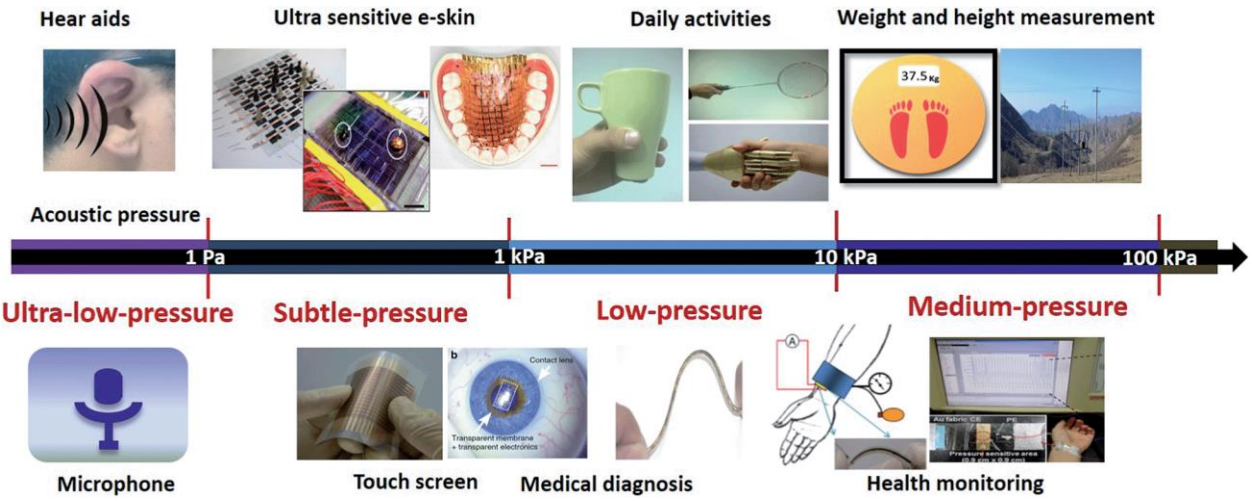

Figure 1.1. Categories of pressure sensors [14]

Using ferroelectret based field effect transistors with the ferroelectret connected to the gate of the transistor, such that the sound of 100 dB which corresponds to an ultra-low pressure of 2 Pa can be measured [16]. In addition, finger touch with 2 kPa in magnitude in pressure could be measured. The uniqueness of this pressure sensor to measure pressure in wide ranges (as low as 2 Pa to 2 kPa or more) was due to the capacitive and piezoelectric property of the ferroelectret used to induce capacitance changes as well as generate a voltage at the gate of the transistor. Pressure

sensors in this range are useful for touch screens, mobile phones as well as e-skin for robotic applications and prosthetic skins [17-20].

Pressure sensors in the medium range are used to measure blood pressure and for pulse monitoring and environmental pressure [21, 22]. One of such pressure sensor is a carbon nanotube transistor based pressure sensor used to measure environmental pressure in this range. The output current change of the transistor could measure air pressure on the tire of a vehicle as well as to monitor the wear and tear of the tire. Pressure sensors in this regime could be used to monitor human walking steps and positions [23, 24]. These could have huge potential in societies with an aging population to keep track of the wellbeing of adults in care homes. For example, as bed sensors to monitor their sleeping patterns and sensor sheets embedded in floor mats to monitor their movements [25].

1.1.2. Transduction mechanism

According to their transduction mechanisms, pressure sensors are classified into there (3) as seen in Figure 1.2.

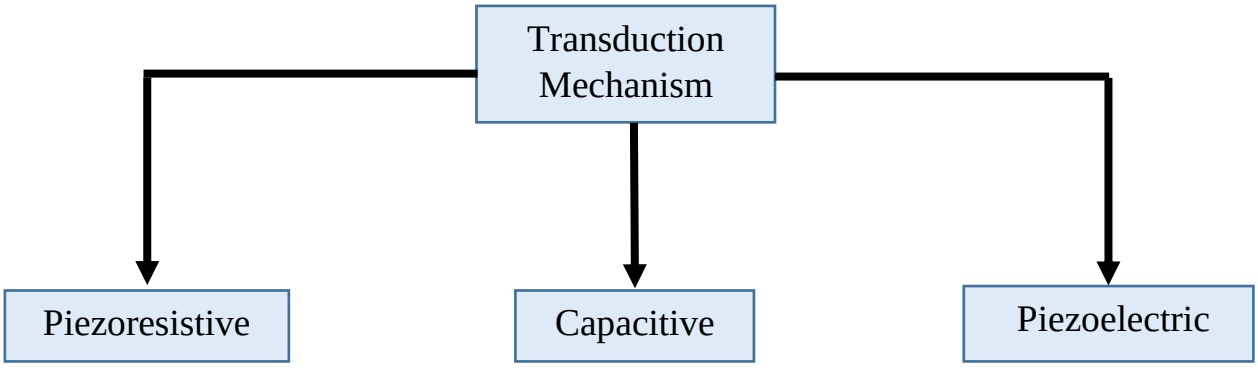

Figure 1.2. Transduction mechanism classification

Piezoresistive sensors

Exerting pressure to a piezoresistive material sandwiched between metal electrodes gives rise to the change in contact resistance (R_c) between the two materials. This change in resistance leads to an output signal change, which could be current. Figure 1.3(a) shows the piezoresistive sensor that is in between two electrodes. When compressed, the piezoresistive material which in this case an organic semiconducting material, PEDOT: PSS (poly (3,4-ethylenedioxythiophene)-poly(styrenesulfonate)) on a compressible PDMS layer of pyramidal structure. Figure 1.3 (b) show the chemical structure of PDMS. The current across the metal electrodes increases even further because of contact area of the piezoresistive electrode to the bottom metal electrode. The change in contact resistance solely depends on the magnitude of the pressure and the contact area change between the two materials. An ultra-sensitive pressure sensor was demonstrated using elastic microstructured film, polydimethylsiloxane (PDMS) sandwiched between two electrodes [26]. When pressure is exerted on the device, the hollow-sphere material increases in the contact area with the electrodes, therefore changing the resistance measured.

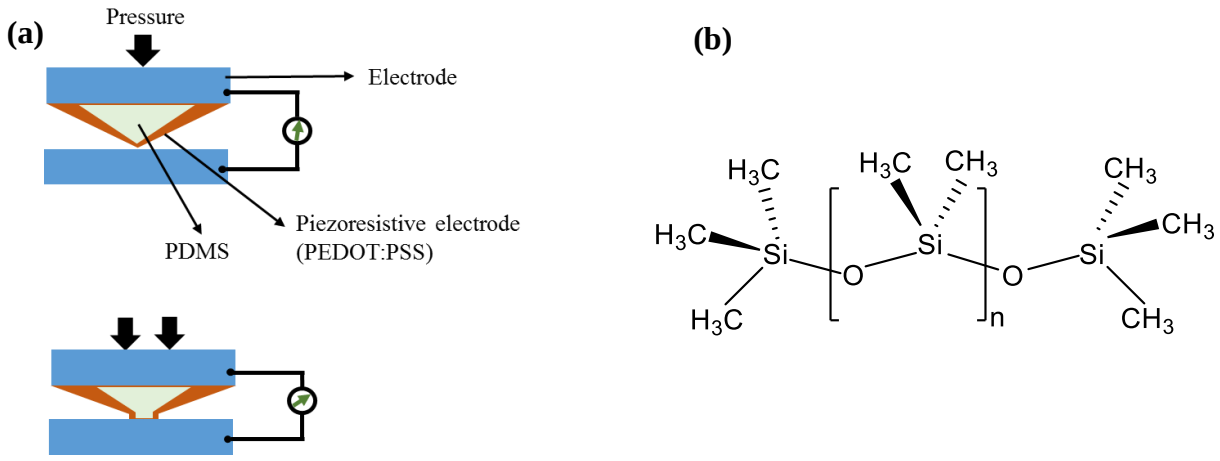

Fig. 1.3 (a) Schematic diagram of a piezoresistive sensor (b) chemical structure of PDMS

Capacitive sensors

When voltage is applied to the parallel plates (Au) of a capacitor, equivalent charges are stored in the material. As long as the voltage is applied, the material stores these charges. Applying pressure to the sensor causes the deflection of its parallel plates with *A*, and the capacitance *C* changes in inverse proportion to the change in thickness, *d* of the sensing material (see Fig 1.4.). The capacitance change is given by the equation below:

$$C = k\varepsilon A/d$$

Where *k*, is relative permittivity of the material and ε is the permittivity of free space. One way to measure the signal output from capacitive sensors is by integrating them with transistors.

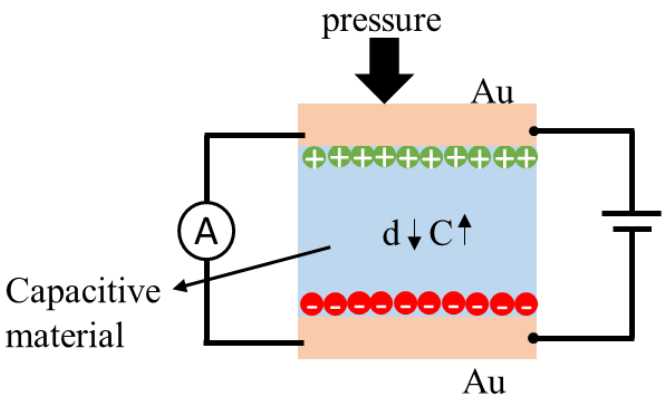

Figure 1.4. Schematic diagram of a capacitive sensor

The output signal generated from the capacitance change modulates the output drain current of the transistor. One capacitive material used widely for sensing application is polydimethylsiloxane (PDMS). When used in conjunction with an OFET device as gate dielectric, the capacitance changes when the PDMS gate dielectric film is compressed leading to a corresponding change in the gate potential. For microstructure PDMS gate dielectric, air is displaced when compressed leading to a higher change in capacitance in comparison to a PDMS film [21, 27].

Piezoelectric sensors

When pressure is exerted on piezoelectric materials, voltage or charges are generated due to dipole moments in the material (in blue), leading to separation of equal and opposite charges on the electrodes (Au in this case) (Fig. 1.5.). The output signal from the sensor could be measured via a wire connected to gate electrodes of a transistor or an oscilloscope. One unique application of piezoelectric materials is that they could be used for self-powered sensors [28-30]. To amplify signals generated by piezoelectric materials, they are integrated with transistors [31- 33]. The transistor semiconducting channel has charge carriers which are modulated by charges/voltage generated by the piezoelectric layer when compressed. Voltage emanating from them could modulate the threshold voltage of OFETs, just like the top-gate voltage from conventional-dual gate OFETs [34]. They are mostly used for measuring dynamic pressure.

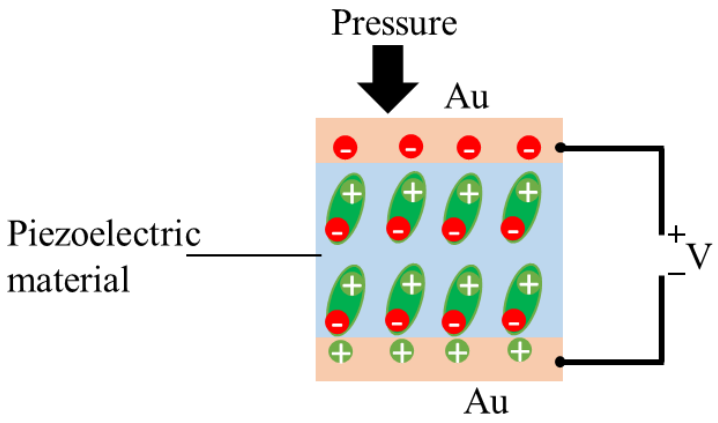

Figure 1.5. The schematic diagram of a piezoelectric sensor

Basic Parameters of Pressure Sensor

Key parameters to assess the performance of a pressure-sensing device include, limit of detection, sensitivity, response time, linearity and stability.

The **sensitivity** (S) is the output signal divided by pressure. For example, if the output signal is current, the change in current, (ΔI) with respect to the minimum current (I_0) is divided by pressure, (P):

$$S = \frac{\Delta I / I_0}{P} \quad \ldots\ldots\ldots\ldots\ldots\ldots\ldots\ldots (1)$$

Limit of detection is the lowest pressure that gives the most distinguishable change in the output signal.

Linearity depicts the level of performance of a pressure sensor in correlation to a specified measured quantity. For example, in OFET based pressure-sensing devices, the linear relation between the pressure magnitude and threshold voltage is a typical form of measuring linearity.

Response time is the time consumed during pressure exertion and release processes. The **stability** of the output signal at a particular pressure magnitude is vital.

These parameters are essential to determine the quality of organic pressure sensors; however, my research focuses on the sensitivity of the pressure-sensing device and its operating voltage. This is because the operating voltage determines the power consumption of pressure sensing device.

1.3. Organic field effect transistors (OFETs) used as transducers for pressure-sensing devices

Organic single crystals [35], small molecules [36, 37], and polymers [38] are semiconductors that have been used as active layers in OFET devices. These OFETs have in turn been utilized as read-out elements in pressure-sensing devices. Organic semiconducting could either be single crystals or in particle form which can be easily dissolved in organic solvents.

For physical vapor transport grown organic crystals such as rubrene, with extremely low trap states exists between the semiconductor/dielectric interfaces, therefore could turn-on at low voltages [39, 40]. This is because the charge carriers fill up the density of states in the channel region, therefore the few trap states are easily filled with low gate potential. In addition, they have low subthreshold swing, (*SS*) of 65 mV/dec, which is near the theoretical limit of 58 mV/Dec as well as high mobility, 15 $cm^2/V.s$. The crystal is usually transferred between the source-drain contact to create a semiconducting channel. Growing the organic crystals and the process of moving it to the substrate to complete the device fabrication is not adaptable for the high-throughput roll-to-roll fabrication of OFETs.

Stefan *et al.* used rubrene based OFET with microstructured polydimethylsiloxane (PDMS) as the sensing layer to develop pressure sensor [27]. Fig. 1.6(a) shows the device structure of the pressure sensing device with a top-gate ITO/PET electrode. The change in capacitance of the PDMS when pressure load is exerted on it gave rise to the change in drain current. Therefore, increasing the pressure load lead to an observed change in drain current as seen in Fig. 1.6 (b). The device sensitivity is 0.55 kPa^{-1}. The air voids between the microstructure of the film contributed to the capacitance change. However, the pressure-sensing devices were fabricated on rigid Si/SiO_2 substrates, which is not flexible. In addition, the single rubrene crystals are not compatible with

bendable pressure sensors, therefore the device cannot be applicable for skin-touch wearable devices.

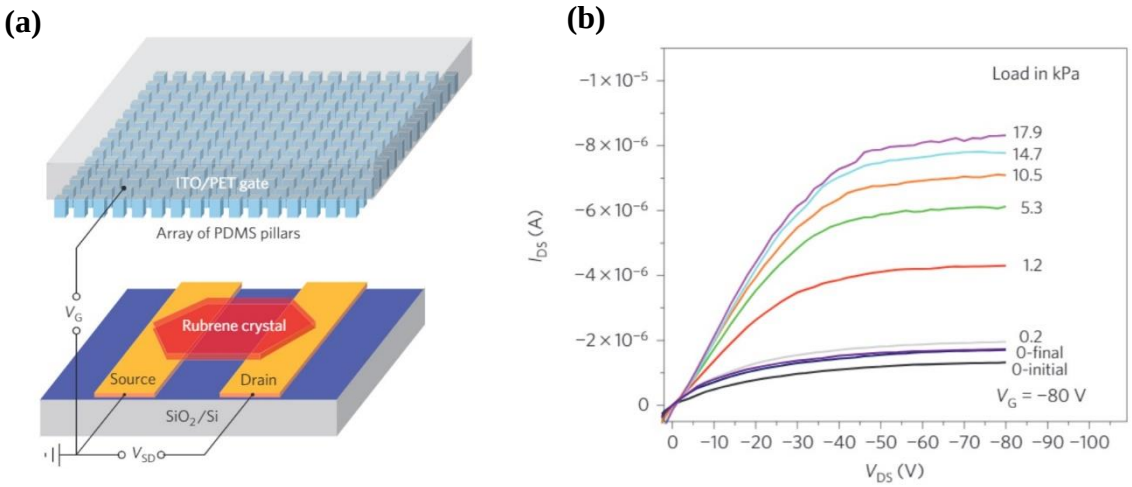

Figure 1.6(a) Rubrene crystal OTFT device and the microstructured PDMS pressure sensing layer (b) change in output curve in response to pressure load [27]

A conjugated polymer (polyisoindigobithiohene-siloxane, (PiI2T-Si)) based OFET device with mobility greater than 1 cm^2/V.s, was used as a read-out element for pressing sensing [21].

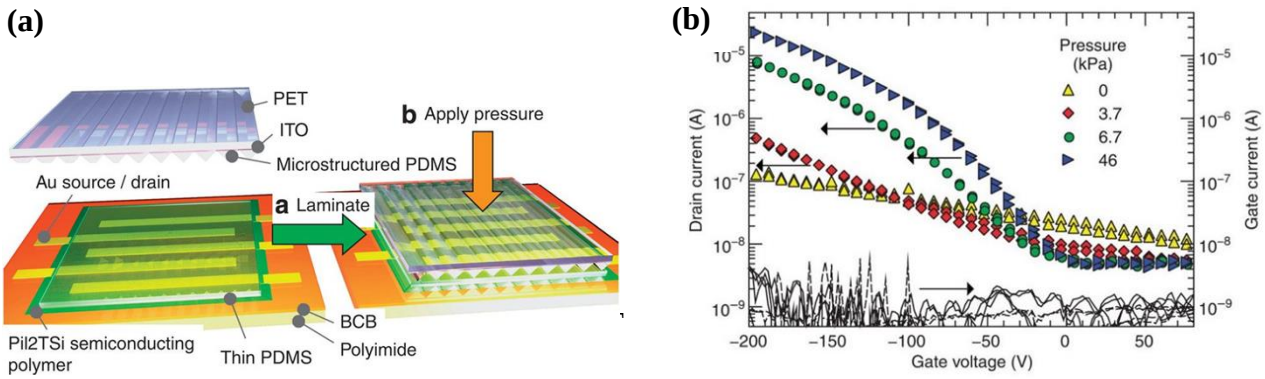

Figure 1.7. (a) Device configuration of the pressure sensitive transistor (b) change in transfer curve with response to pressure load [21].

Unlike the rubrene single crystal-based pressure sensor described above, the device here was flexible (see Fig. 1.7.). This is because of the microstructured PDMS film on a flexible PET-ITO substrate and semiconducting layer deposited on a flexible substrate. The device sensitivity

increased due to capacitance change when pressure was exerted on it. As can be seen in Fig. 1.7, when the pressure load was increased, the threshold voltage shifted to the left and the OFF current reduced. However, the number of trap states formed at the dielectric interface makes it impossible to achieve low-voltage operations (<10 V) using these semiconducting polymers; thus leading to an operation voltage of -200 V. In addition, the mobility of the device is dependent on processing temperature (> 100 °C) [41], which is not suitable for plastic substrates with glass transition temperatures that are not above 100 °C. The device shows a maximum sensitivity of 8.4 kPa^{-1} at pressure load of 8 kPa. High sensitivity result achieved by this device in comparison to the rubrene based pressure sensor was caused by the triangular microstructure of the PDMS dielectric interface, which gave rise to a high change in capacitance when pressure load was exerted on it.

Using dinaphtho[2,3-b:2',3'-f]thieno[3,2-b]thiophene (DNTT) as semiconducting layer, resistive pressure sensors have been developed [42]. The organic transistor had high mobility between 1 – 2 cm^2/V.s. For the fabrication of the pressure sensing device, the Au source-drain electrodes

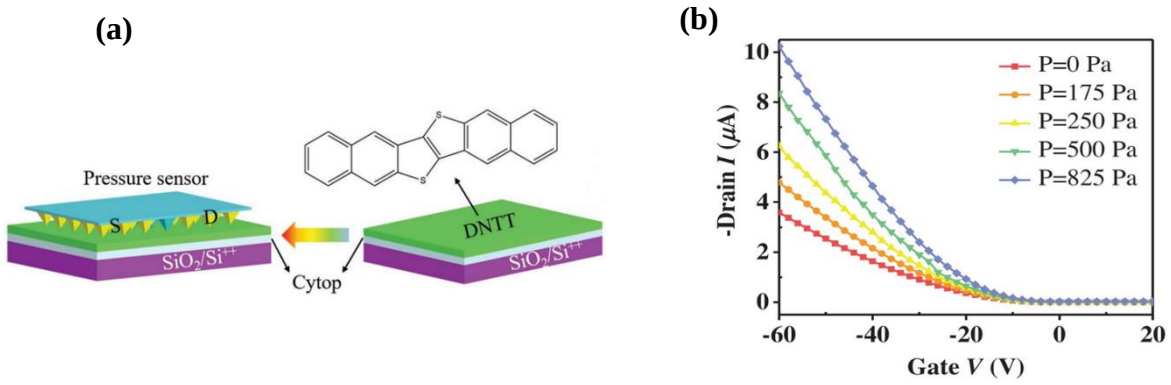

Figure 1.8 (a) schematic diagram of the piezoresistive sensor (b) change in transfer curve with response to pressure load [42]

were deposited on the pyramidal microstructure of the PDMS sensing layer as seen in Fig. 1.8(a). The device operation was based on the change in channel and contact resistances in response to

pressure load. The change in resistance led to an increase in drain current as the pressure load is increased as seen in Fig. 1.8(b). However, the drive voltage used for this device was quite high (60 V); therefore, a battery cell cannot power the sensor. In addition, the Si-based devices are rigid, therefore cannot be bent.

Elsewhere, polymers of diketopyrrolopyrrole terthiophene (PDPPT3) as organic semiconductors for OFET devices were used in a suspended gate pressure sensor configuration (see Fig. 1.9 (a)) [43]. The mobility of OFETs based on these organic semiconductors is higher than 1 $cm^2/V.s$. Similar to PiI2T-Si based OFET, they require high operation voltages, 60 V. When pressure is applied to the suspended gate, it makes contact with the poly(perflurobutenylvinylether) (CYTOP) dielectric layer. The magnitude of pressure load on the suspended gate displaces air which has a low dielectric constant of 1 caused a considerable change in capacitance; the capacitance change is huge, hence the reason for the high sensitivity, 192 kPa^{-1} recorded by this device.

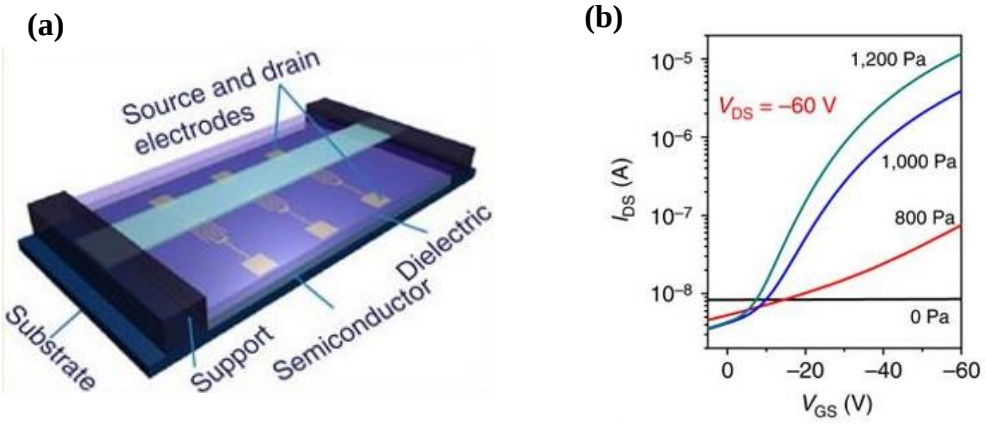

Figure 1.9. (a) Schematic diagram of a suspended gate organic transistor (b) change in transfer curve with response to pressure load [43]

To reduce the operation voltage of OFETs, TIPS-pentacene organic semiconductors have been of interest because they form crystals with a dielectric interface; therefore, could record mobility > 1 $cm^2/V.s$. When blended with insulating polymers such as polystyrene, they could be easily solution-processed and crystallized in <= 100 °C annealing temperature [34, 36, 44]. However, OFETs based on this semiconducting blend has not been used for pressure sensing applications. Possibly, because of the difficulty required to achieve high mobility. For example, a pressure

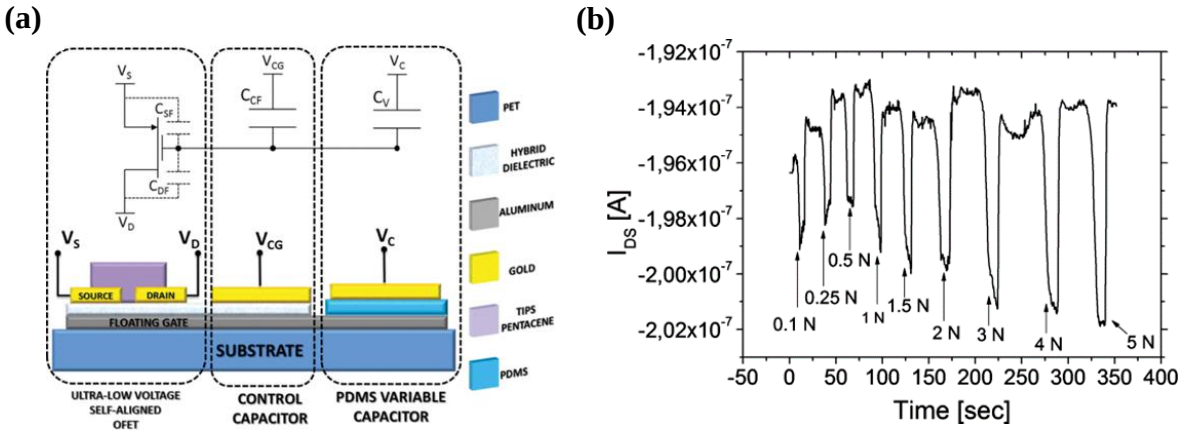

Figure 1.10 (a) schematic diagram of the pressure modulated OFET (b) output current versus time for the PMOFET [45]

sensor with configuration comprising of a low-voltage OFET and PDMS film attached to a floating gate has been reported (see device configuration in Fig. 1.10 (a)) [45]. When pressure is exerted on the PDMS film, its capacitance changes, causing charges on the floating gate to be dispersed such that the mobile charge carriers in the OFET's semiconducting channel are modulated by this process. However, the device recorded a small change in drain current ($\Delta I/I_o$), close to 0.04 at pressure magnitude of 78 kPa, where ΔI is the drain current change with pressure exerted on the film and I_o is the drain current at minimum pressure. The small change in drain current observed was caused by the small change in capacitance of the PDMS film.

Using a PVDF piezoelectric layer in connection to a floating gate organic FET, dynamic force in range 0 to 3.5 N was measured by the change in drain current (see Fig. 1.11) [46]. The operation voltage of the organic transistor was quite low, -3 V. However, the performance of the device is limited by parasitic capacitance caused by the proximity of the source, drain, and sensing layer. In summary, the sensitivity of pressure sensing devices, do not solely depend on the performance

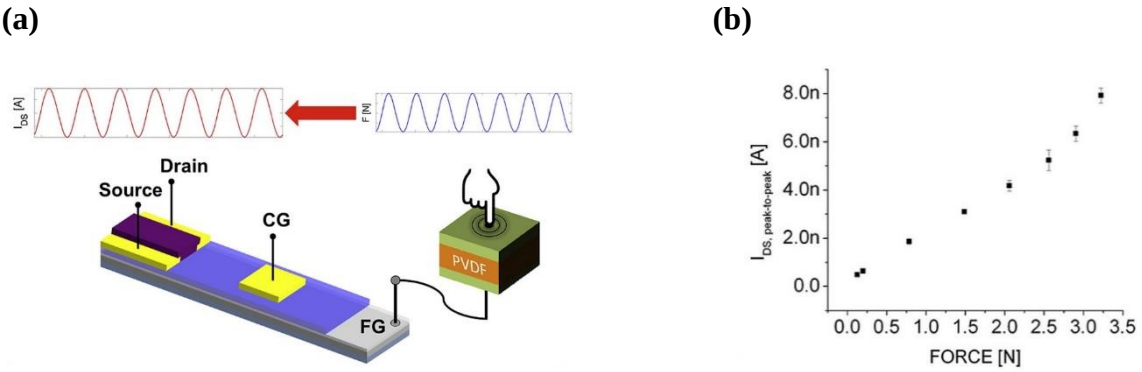

Figure 1.11 (a) schematic diagram of the organic charge modulated FET with PVDF as sensing membrane (b) drain current change with respect to force [46]

of the OFET, but also on the sensing layer used to modulate the charge carriers in the active layer of these OFETs. The area of the sensing layer was not given, therefore a graph of drain current against pressure couldn't be replotted.

Table 1 summarises the performance parameters of the OFET based pressure-sensing devices mentioned in this chapter.

Table 1. Summary of performance of the pressure-sensing devices mentioned

Transduction mechanism	Sensing layer	Operation voltage of OFET	Sensitivity or ($\Delta I/I_0$)	Response time	Linearity	Limit of detection
Capacitive	PDMS film [46]	-3 V	0.04	-	yes	156 kPa
Capacitive	PDMS microstructure [27]		0.55 kPa^{-1}	4 s	yes	3 Pa
Capacitive	PDMS microstructure [21]	-200 V	8.4 kPa^{-1}	<10 ms	yes	-
Capacitive	Air [43]	60 V	192 kPa^{-1}	10 ms	yes	0.5 Pa
Piezoresistive	Conducting channel & source-drain contact [42]	60 V	514 kPa^{-1}	1.8 ms	yes	10 Pa
Piezoelectric	PVDF [46]	-2 V	-	-	yes	300 Pa
Piezolectric	P(VDF-TrFE) [33]	-2 V	7.5 pF/N	7 s	yes	-
Piezoelectric	P(VDF-TrFE) [34]	-5 V	155	-	yes	-

1.4. Current studies on OFET based pressure-sensing devices

Pressure-sensing devices that are flexible, highly sensitive and can operate at low voltages have been of huge of interest. Devices with these properties could drive the display electronics industry forward as well as man-machine interface technologies, i.e., electronic skin for robots.

Research into electronic sensors that can mimic the human skin is currently ongoing [47]. One major drawback of the electronic skin is that they are not as stretchable like the human skin and do not cover large areas. Getting to invent electronic skins that mimic the human skin in all ramifications could have potential applications for the sensing capabilities of robots.

Replacing devices based on Si wafers with organic materials is currently ongoing. One of the primary cause of attraction is the cost required in manufacturing these devices in using these materials in comparison with Si-based devices. However, compared to Si or other crystalline based FETs with field-effect mobility higher than 1000 $cm^2/V.s$ [48], the field-effect mobility for organic based FETs is quite low (< less than 10 cm^2/Vs). Therefore, a need to develop organic insulators and semiconductor materials that would boost the mobility of OFETs is needed.

Reducing the operation voltage of OFETs used as read-out elements in transistors are currently ongoing. The operation voltage of the transistor defines the power consumption of the sensing device. High power consumption required for pressure-sensing devices available today inhibit their application to wearable devices for daily activities; since they cannot be powered by battery cells. Therefore, reducing the power consumption of these sensors is necessary for commercial viability of the devices. One such consideration is to develop high-*k* organic insulators or solution-processed metallic oxides such as ZrO_2 and HfO_2 [49, 50]. This could increase charge carriers induced in the semiconducting channel as well as reduce the operation voltage of the transistor.

Another challenge with using OFET as the read-out element for pressure sensing devices is the lifetime of the transistors as well as its reliability during operation. Therefore, a dire need in developing organic transistors that are reliable and can last as long as Si-based devices are ongoing.

The climate is changing because of greenhouse gas emissions caused by fossil fuels and its byproducts. One way to end greenhouse gas emission into the stratosphere is by developing materials that are eco-friendly and can be readily disposable after their lifetime without causing irreparable harm to the eco-system. Therefore, there is a need to develop bio-friendly materials that are sustainable and degradable for future transistors. Research is ongoing on possible substrates [51, 52], semiconducting [53], insulating materials [54] that are derived directly from the environment.

1.5. Previous research by our group

Integrating a sensing capacitor with a low-voltage OFET, a pressure sensing device was developed [55]. Fig. 1.12(a) is a schematic diagram of the organic pressure sensor. The sensing piezoelectric capacitor was connected to the gate electrode of the OFET; more like an extended gate. The OFET device operated at a low gate voltage of -5 V, and drain voltage of -6 V. The sensing capacitor used was P(VDF-TrFE) film sandwiched between two Al electrodes. The film was polarized by contact poling process with a poling voltage of -1000 V. The dipole moments of the film was oriented parallel the direction electric field from bottom substrate to the top of the film. Applying pressure on the piezoelectric P(VDF-TrFE) film modulated charge carriers in the active layer of the OFET; the drain current decreased 16 times below the original value as seen in Fig. 1.12(b). In addition, change in drain current was shown for the P(VDF-TrFE) film that was unpoled. This suggests that the pressing sensing mechanism of the device was caused by the piezoelectric behavior of the polarized P(VDF-TrFE) film. However, the drawback to this device is that no change in V_{th} was observed, which was due to electrostatic charges which caused electrical noise during measurement.

(a)

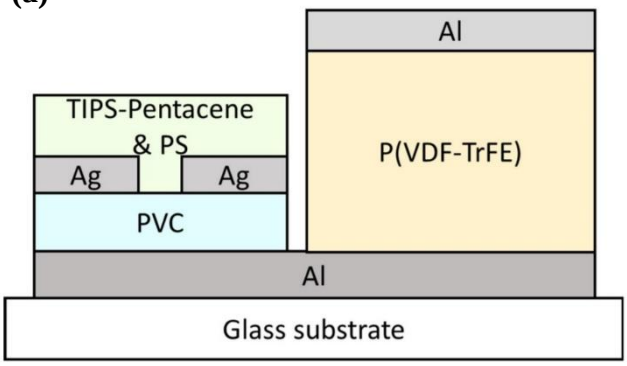

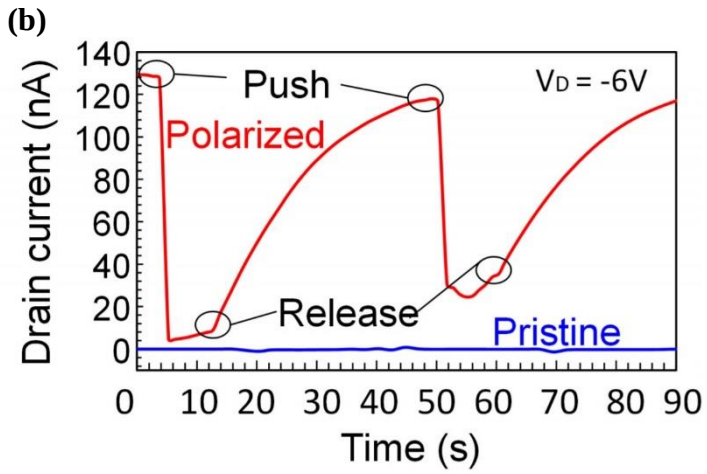

Figure 1.12(a) schematic diagram of the organic pressure sensor (b) drain current response of the OFET integrated with the sensing layer. Red (polarized) blue (pristine or unpolarized) [55].

To mitigate the problem of electrostatic charges caused directly poling the P(VDF-TrFE) film, a novel organic pressure sensor configuration was developed [34]. The same sensing layer as the organic pressure sensor with the extended gate structure was used. However, the piezoelectric layer was fabricated, and then polarized separately from the low-voltage OFET, therefore circumventing the problem of electrostatic charges arising from in-situ poling of the device. Figure 1.13(a) shows the device configuration of the organic pressure sensor called the dual-gate organic pressure sensor.

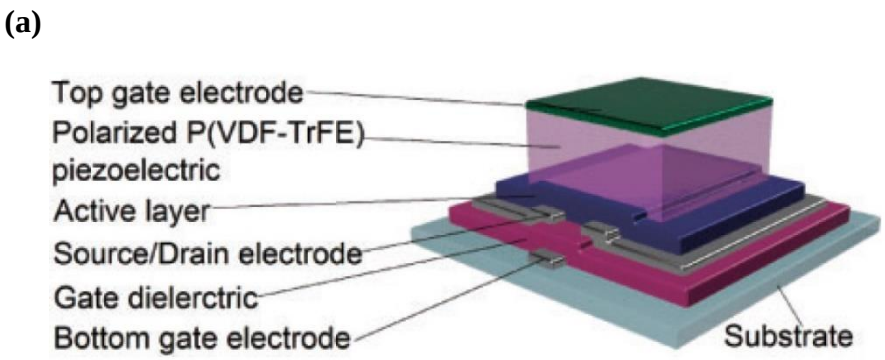

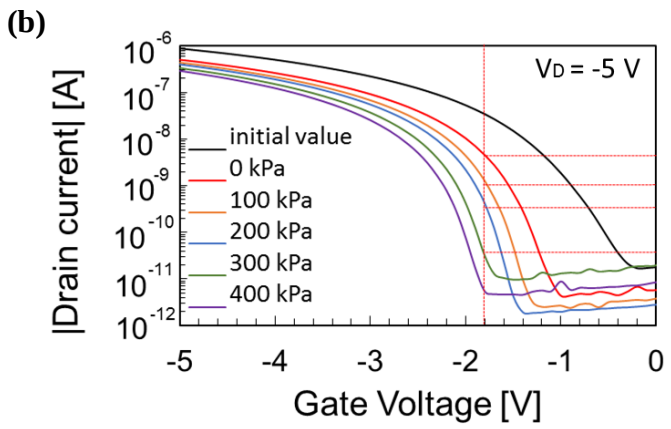

Figure 1.13(a) schematic diagram of the dual-gate organic pressure sensor (b) transfer curve shift with respect to the load [34].

The configuration of the device as seen in Fig. 1.13(a) consists of a poled P(VDF-TrFE) film in connection to the semiconducting film of the read-out element. Exerting pressure on the piezoelectric layer caused a shift in the transfer curve, suggesting that the polarized P(VDF-TrFE) film acted as a top-gate voltage. The left shift of the transfer curve increased based on the magnitude of the pressure load, as seen in Fig. 1.13(b). Significant change of $\Delta I/I_o$ of 155 was achieved when pressure load of 300 kPa was exerted on the device. This research focused on organic pressure sensor performance caused by its operation conditions and sensing potential. Nevertheless, a quantitative explanation, as well as a scientific description of the operation of the devices, is yet to be proven.

1.5. Aims of this study (My research)

This study focuses on the quantitative description of the device operation of a low-voltage dual-gate organic pressure sensor with the following objectives:

- Proposing a scientific explanation for the operation mechanism of the device
- Quantitative clarification of the device's sensing mechanism
- A scientific explanation of the piezoelectric effect caused by the sensing layer to the transfer curve shift observed without pressure load.

To achieve these objectives, the dual-gate pressure-sensing device already reported by the previous student in the laboratory has to be reproduced. To fabricate the dual-gate organic transistor based pressure sensor, a low-voltage bottom-gate OFET was fabricated in **chapter 2** using dielectrics such as poly (vinyl cinnamate) (PVCN) and an environmentally friendly and degradable biopolyamide. The photochemical crosslinking process was carried out to make the PVCN insulator chemically resistant to chlorobenzene solvent while the biopolyamide material was characterized to confirm if it was chemically resistant to chlorobenzene. Using these insulators, the OFETs operated in a low voltage range, 1 V to -5 V, because of the reduced interface traps the dielectrics formed with the TIPS-Pentacene/polystyrene semiconducting blend. The few trap states allowed for charge carriers to fill up the sub-gap density of states thus leading to a small subthreshold slope of values 108 mV/decade for the biopolyamide based OFET and 110 mV/decade for the PVCN based OFET. The mobility of the OFETs was 0.27 cm^2/V and 0.18 cm^2/V for the biopolyamide and PVCN respectively. The results obtained using the biopolyamide increases the prospects of eco-friendly organic transistors available for use in the nearest future. In **chapter 3**, a dual-gate pressure sensor device was successfully fabricated. A linear graph of the pressure load against V_{th} was obtained. The transfer curve shifts by the pressure load were similar

to conventional dual-gate OFET. Therefore, in **chapter 4**, a low-voltage dual-gate OFET using CYTOP as top-gate dielectric was successfully fabricated. From these results, the quantity of charges on the polarized P(VDF-TrFE) film was estimated.

In **Chapter 5**, a quantitative analysis to get the polarized P(VDF-TrFE) piezoelectric constant, d_{33} using the change in threshold voltage shift, (V_{th}) obtained from the transfer characteristics shift results, results from a conventional dual-gate OFET was carried out. In addition, d_{33} quantitatively determined was in the same order with directly measured value, 53 pC/N. **Chapter 6**, the surface charges on the polarized PVDF-TrFE layer required to cause the initial V_{th} shift, with respect to the magnitude of electric field used to polarize the P(VDF-TrFE) layer was quantified. **Chapter 7** summarizes the results achieved in the previous chapters, future research as well as prospective applications of this work.

References

[1] P. Rosa, A. Câmara, and C. Gouveia, Open J. Internet Things, **1** (2015) 16–36.

[2] Y. Zhan, Y. Mei, and L. Zheng, J. Mater. Chem. C, **2** (2014) 1220–1232.

[3] A. Zanella, N. Bui, A. Castellani, L. Vangelista, and M. Zorzi, IEEE Internet Things. J., **1** (2014) 22–32.

[4] V.R. Feig, H. Tran, and Z. Bao., ACS Cent. Sci. **4** (2018) 337-348.

[5] M. Berggren, D. Nilsson, and N. D. Robinson, Nat. Mater. , **6** (2007) 3–5.

[6] A. C. Arias, J. D. MacKenzie, I. McCulloch, J. Rivnay, and A. Salleo, Chem. Rev., **110** (2010) 3–24.

[7] G. H. Gelinck, H. Edzer, A. Huitema, E. van Veenendaal, E. Cantatore, L. Schrijnemakers, J. B. P. H. vanderPutten, T. C. T. Geuns, M. Beenhakkers, J. B. Giesbers, B.-H. Huisman, E. J. Meijer, E. MenaBenito, F. J. Touwslager, A. W. Marsman, B. J. E. vanRens, and D. M. deLeeuw, Nat. Mater. , **3** (2004) 106–110.

[8] L. Feng, W. Tang, J. Zhao, R. Yang, W. Hu, Q. Li, R. Wang & X. Guo., Sci. Rep., **6** (2016) 20671

[9] Z. A. Lamport, H.F. Haneef, S. Anand, M. Waldrip and O. D. Jurchescu., J. Appl. Phys. ,**124** (2018) 071101.

[10] B. Geffroy, P. le Roy, C. Prat., Polym. Int. **55** (2006) 572-582.

[11] M. Wright, A. Uddin., Sol. Energy Mater, Sol. Cells., **107** (2012) 87-111

[12] F. Maita, L. Maiolo, A. Minotti, A. Pecora, D. Ricci IEEE Sens. J., **15** (2015) 3819-3826

[13] S. Hannah, A. Davidson, I. Glesk, D. Uttamchandani, R. Dahiya, H. Gleskova., Org. Electron **56** (2018) 170-177.

[14] Y. Chen, B. Lu, Y. Chen, & X. Feng., Sci. Rep., **5** (2015) 11505

[15] Y. Zang, F. Zhang, C-an Di, D. Zhu. Mater. Horiz., **2** (2015), 140- 156

[16] I. Graz, M. Kaltenbrunner, C. Keplinger, R. Schwodiauer, S. Bauer. Appl. Phys. Lett. **89**, (2006) 073501

[17] S. Gong, W. Schwalb, Y. Wang, Y. Chen, Y. Tang, J. Si, B. Shirinzadeh and W. Cheng, Nat. Commun., **5** (2014) 3132

[18] L. Pan, A. Chortos, G. Yu, Y. Wang, S. Isaacson, R. Allen, Y. Shi, R. Dauskardt and Z. Bao, Nat. Commun., **5** (2014) 3002.

[19] A. Chortos, J. Liu and Z. Bao., Nat. Mater., **15** (2016) 937-950.

[20] M. L. Hammock, A. Chortos, B. C. Tee, J. B. Tok and Z. Bao, Adv. Mater., **25** (2013) , 5997-6038.

[21] G. Schwartz, B.C.-K. Tee, J. Mei, A.L. Appleton, D.H. Kim, H. Wang, Z. Bao, Nat. Commun. **4** (2013) 1-8

[22] J. B. Andrews, J. A. Cardenas , C. J. Lim, S.G. Noyce, J. Mullett, A. D. Franklin., IEEE sensors Journal., **18** (2018) 7875-7880

[23] Y. Watanabe, S. Uemura and S. Hoshino., Jpn. J. Appl. Phys., **53** (2014) 05HB15

[24] J. Suutala and J. Röning. INFORM FUSION. **9** (2008) 21-40

[25] A. Arcelus, I. Veledar, R. Goubran, F. Knoefel, H. Sveistrup, and M. Bilodeau, IEEE Trans. Instrum. Meas., **60** (2011) 1732

[26] C. L. Choong, M. B. Shim, B. S. Lee, S. Jeon, D. S. Ko, T. H. Kang, J. Bae, S. H. Lee, K. E. Byun, J. Im, Y. J. Jeong, C. E. Park, J. J. Park and U. I. Chung, Adv. Mater., **26** (2014) 3451.

[27] S.C.B. Mannsfeld, B.C.K. Tee, R.M. Stoltenberg, C.V.H.H. Chen, S. Barman, B.V.O. Muir, A.N. Sokolov, C. Reese, Z. Bao. Nat. Mater. **9** (2010) 859-864.

[28] F.R. Fan, W. Tang, and Z.L. Wang. Adv. Mater. , **28** (2016) 4283-4305.

[29] K. I. Park, et al. Adv. Mater., **26** (2014) 2450-2450.

[30] L. Lin, Y. Xie, S. Wang, W. Wu, S. Niu, X. Wen and Z. L. Wang, ACS Nano., **7** (2013) 8266

[31] R.S. Dahiya, G. Metta, M. Valle, IEEE Trans. Ultrason., Ferroelectr., Freq. Control., **56** (2009) 2.

[32] F. Maita, L. Maiolo, A. Minotti, A. Pecora, D. Ricci, G. Metta, G. Scandurra, G. Giusi, C. Ciofi, and G. Fortunato. IEEE Sensors Journal., **15** (2015) 3819-3826

[33] S. Hannah, A. Davidsona, I. Glesk, D. Uttamchandani, R. Dahiya, H. Gleskova. Org. Electron., **56** (2018) 170-177

[34] Y. Tsuji, H. Sakai, L. Feng, X. Guo and H. Murata. Applied Physics Express., **10** (2017) 021601

[35] R. W. I. de Boer, T.M. Klapwijk, and A. F. Morpurgo., **83** (2003) 4345-4347.

[36] J. Kang, N. Shin, D. Y. Jang, V. M. Prabhu, and D.Y. Yoon., J. Am. Chem. Soc., **130** (2008), 12273–12275

[37] D. K. Hwang, et al., J. Mater. Chem., **22** (2012), 5531-5537

[38] K. Takagi, T. Nagase, T. Kobayashi, T. Kushida and H. Naito., JJAP. **54** (2015) 011601.

[39] R.A. Laudise, C. Kloc, P. G. Simpkins, T. Siegrist. J. Cryst Growth., **187** (1998) 449-454

[40] B. Blulle, R. Hausermann, and B. Batlogg. Phys. Rev. Appl. **1** (2014) 034006

[41] J. Mei, D. H. Kim, A.L. Ayzner, M.F. Toney, Z. Bao J. Am. Chem. Soc., **133** (2011), 20130–20133

[42] Z. Wang, et al., Adv. Mater. **31** (2019), 1805630

[43] Y. Zang, F. Zhang, D. Huang, X. Gao, C. Di, D. Zhu, Nat. Commun., **6** (2015) 6269.

[44] L. Feng, W. Tang, X. Xu, Q. Cui, and X. Guo, IEEE Electron Device Lett. **34** (2013) 129 - 131.

[45] S. Lai, P. Cosseddu, A. Bonfiglio and M. Barbaro, IEEE Electron Device Letters., **34** (2013) 801-803.

[46] A. Spanu, L. Pinna, F. Viola, L. Seminara, M. Valle, A. Bonfiglio, P. Cosseddu., Org. Electron., **36** (2016), 57-60.

[47] A. Chortos, J. Liu, Z. Bao. Nat. Mater., **15** (2016), 937-950.

[48] M.C. Lemme, T.J. Echtermeyer, M. Baus, B. N. Szafranek, J. Bolten, M. Schmidt, T. Wahlbrink, H. Kurz., SOLID STATE ELECTRON., **52** (2008), 514-518.

[49] R. P. Ortiz, A. Facchetti, and T.J. Marks.,**110** (2010), 205-239

[50] J. Heo, S.Y. Park, J. W. Kim, S. Song, Y.L. Yoon, J. Jeong, H. Jang, K.T. Lee, J. H. Seo, B. Walker, J. Y. Kim., Adv. Funct. Mater., **28** (2018) 1704215

[51] D.-H. Kim, J. Viventi, J.J. Amsden, J. Xiao, L. Vigeland, Y-S. Kim, J. A. Blanco, B. Panilaitis, E.S. Frechette, D. Contreras, D. L. Kaplan, F.G. Omenetto, Y. Huang, K-C. Hwang, M. R. Zakin, B. Litt & J. A. Rogers., Nat. Mater., **9** (2010) 511

[52] C. J. Bettinger, Z. Bao., Adv. Mater., **22** (2010) 651

[53] R. Burch, Y. Dong, C. Fincher, M. Goldfinger, P. Rouviere., Synth. Met., **146** (2004), 43-46

[54] J.-W. Chang, C.-G. Wang, C.-Y. Huang, T.-D. Tsai, T.-F. Guo, T.-C. Wen., Adv. Mater., **23**(2011) 4077-4081

[55] H. Sakai, Y. Tsuji, H. Murata. IEICE TRANS. ELECTRON., **E100–C** (2017) 126-129.

CHAPTER 2 || LOW-VOLTAGE ORGANIC FIELD-EFFECT TRANSISTOR*

In this chapter, low-voltage organic field-effect transistors (OFET) were fabricated and characterized using poly (vinyl cinnamate) (PVCN) and novel biopolyamide as dielectric layer. The biopolyamide surface properties and resistance to chlorobenzene was characterized. The OFET performance parameters with poly (vinyl cinnamate) as dielectric are: μ = 0.18 cm^2/Vs, V_{th} = -0.15 V, on/off ratio = 1.13 × 10^6, *SS* = 125 mV/decade. While the performance parameters for devices with the biopolyamide as dielectric are: μ = 0.27 cm^2/Vs, V_{th} = 0.18 V, on/off ratio = 9.3 × 10^5, *SS* = 108 mV/decade.

*"Biopolyamide as gate dielectric for low-operation voltage solution-processed organic field-effect transistors" (manuscript in preparation)

2.1. Introduction

2.1.1. Poly (vinyl cinnamate) as a dielectric for low voltage OFET

The dielectric plays a significant role in reducing the operation voltage of OFET devices fabricated by solution processes. From the subthreshold swing, *SS* equation (1), it is possible to reduce the gate potential by either increasing the capacitance of the gate dielectric, in this case using high-*k* dielectrics. Since high-*k* dielectrics have large charge density, the charges easily fill-the trap states allowing low V_{th} to be achieved, hence low-voltage operation of the transistor. However, some high-*k* dielectrics may easily be polarized by an electric field leading to energetic disorder and localized states at the semiconducting interface [1-5].

$$SS = \text{In } 10.\ k_b T/q\ (1 + C_{ch}/C_G)$$

Where k_b is the Boltzmann's constant, T is the temperature, C_G is the gate capacitance, q is the electron charge, C_{ch} is the effective channel capacitance. The dipoles formed at the dielectric/semiconducting layer interface causes a broadening of the density of state leading to many trap states; leading to an increase in threshold voltage [6]. In addition, reducing the insulating material thickness of increases the capacitance of the dielectric layer. This causes an increase in charge density required to fill the trap states, therefore leading to lower V_{th}. The most common polymers used as gate dielectrics in OFET are poly (4-vinyl phenol) and poly (vinyl alcohol) [7, 8]. However, the hydroxyl group present in these polymers make them unsuitable: they form dipoles, which leads to slow polarization in the bulk of the gate dielectric [9]. In addition, high gate leakage current and hysteresis are caused by numerous trapping sites formed at the interface. Reducing gate leakage current requires curing, which may add to the fabrication process, hence additional time to complete the device fabrication. PVCN is a low-*k* polymer with reduced

hydroxyl groups. It does not require thermal crosslinking process making it suitable for high-throughput manufacturing processes. However, photocrosslinking is vital to achieving a low-leakage gate current. Crosslinking makes the polymers chemically resistant to organic solvents. The process by which the moieties of the polymer become linked together is known as 2+2 cycloaddition (Fig. 2.1.), which leads to an increase in the breakdown field of the dielectric in comparison to pristine films [10]. In addition, adequately crosslinked PVCN films are patternable using lithography processes.

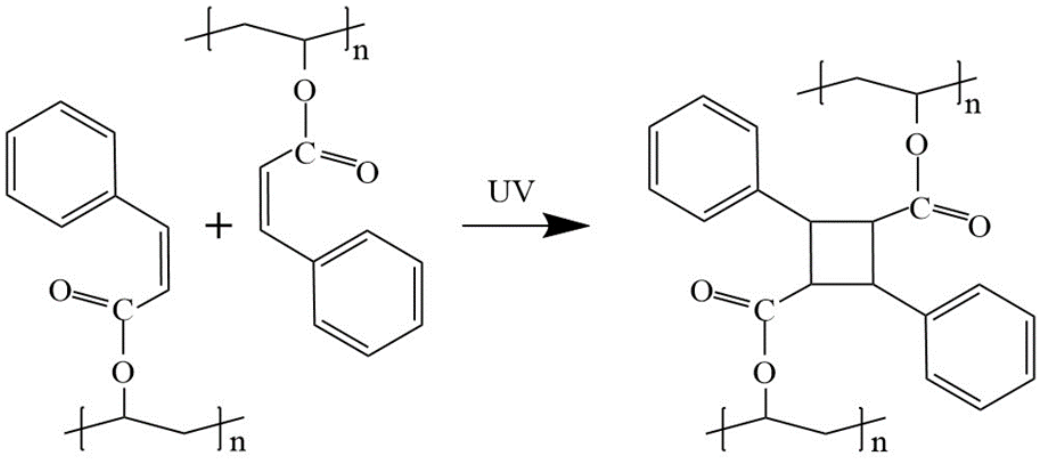

Fig. 2.1. Chemical structure of poly (vinyl cinnmate) (left) and photocrosslinked poly (vinyl cinnmate) (right)

In this chapter, PVCN film 300 nm in thickness was used as a dielectric for the OFET device. A low-voltage of -5 V was enough to induce holes in the dielectric/semiconductor interface of the OFET. The device operation was hysteresis-free indicating the absence of hydroxyl ions.

A blend of TIPS-Pentacene (small molecule) and polystyrene (polymer) was used as the semiconducting material. Figure 2.2(a) & (b) show the chemical structure of TIPS-Pentacene and polystyrene respectively. The reason for blending the acene with the polymer is to improve solution deposition process. Jihoon Kang *et al*. compared the use of TIPS-Pentacene/polymer blend to TIPS-pentacene as the semiconducting layer for OFET device, the mobility of the blend

film, 0.3 cm^2/Vs was higher in comparison to only TIPS-pentacene, 0.05 cm^2/ Vs [11]. This was likely due to a change in the physical and chemical structure of the blend with the dielectric interface.

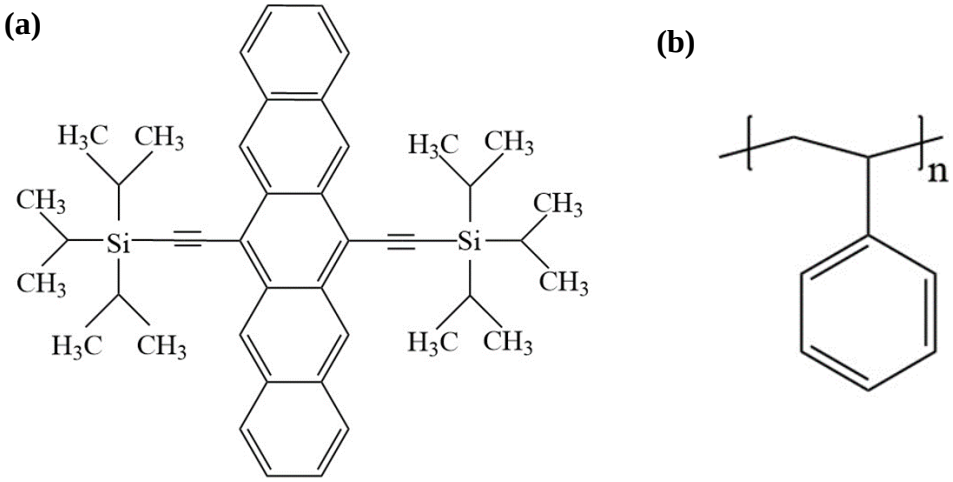

Figure 2.2. Chemical structure of (a) TIPS-pentacene (b) Polystyrene

In addition, the TIPS-pentacene/polystyrene blend forms a tri-layer film, with TIPS-pentacene at the interface of the bottom dielectric and top dielectric (in the case of a dual-gate OFET) and the polymer in the middle [11].

2.1.2. Biopolyamide as dielectric for low-voltage OFET

The advantages of using biopolymer materials for OFET devices are numerous: they are eco-friendly, biodegradable and renewable. However, they are mostly hydrophilic which makes them unsuitable for use in water-sensitive devices. In addition, their low surface energy makes it uneasy to use them for solution-processed organic semiconductors, when used as a bottom-gate dielectric layer. Biomaterials such as chicken albumen, silk fibroin, cross-linked DNA have been utilized as gate dielectrics for OFETs [12-15]. However, the use of biomaterials as dielectric for OFET based on organic semiconducting blends of small-molecules and polymers, deposited by solution process is yet to be reported. These semiconducting blends of organic materials have been

deposited on OFET devices based on low-*k* organic dielectric based such as PVCN that are resistant to organic solvents.

In this section, we report an ultrastrong, transparent and thermally stable bio-based polymer (polytruxillamides) as the dielectric layer in an all solution-processed low voltage OFET with negligible hysteresis and excellent electrical properties. Figure 2.3 shows the chemical structure of the biopolyamide

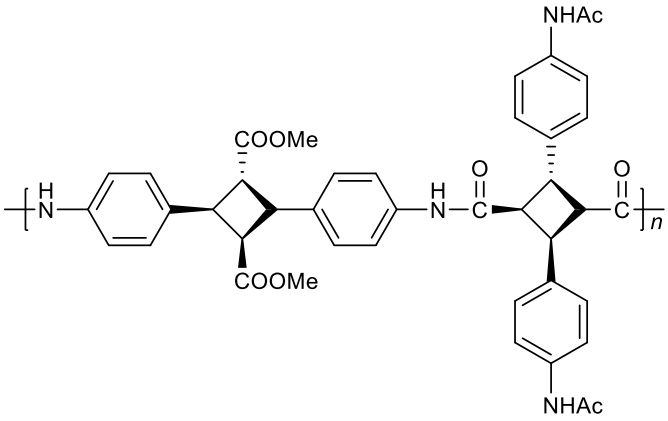

Fig. 2.3. Chemical structure of biopolyamide

This biopolyamide was synthesized from 4-aminocinnamic acid monomer, which was genetically engineered from glucose [16]. To save time during fabrication, this material did not require crosslinking to reduce the gate leakage current as observed in some polymers used as dielectric in OFETs. When annealed, the biopolyamide film is chemically impervious to common organic solvents such as chlorobenzene. Similar to PVCN, a voltage of -5 V was sufficient to modulate the field effect of the channel. In addition, the operation showed negligible hysteresis and low-gate leakage current of $< 10^{-9}$A. This may be due to the absence of hydroxyl groups and the high glass transition temperature of 273 °C of the material. In contrast to PVCN, this material does not require a crosslinking process during device fabrication, therefore reduces the complexity of the

fabrication process. V_{th} of the device was low (-0.85 V), indicating that the gate potential was sufficient to induce charges to fill the trap states at the semiconducting blend/dielectric interface.

In this chapter, the fabrication process and characterization of a low-voltage OFET was done using PVCN and a novel biopolyamide material as insulators. The OFET devices were characterized to as read-out element for low-voltage pressure sensing devices in the next chapter.

2.2. Experimental Methods

The glass substrates were cleaned in acetone for 5 minutes to remove organic dirt and contaminants, then in IPA for 10 minutes to remove the residual Acetone on the glass substrate. The glass substrates surface were further cleaned to remove any residual contaminants using a UV ozone cleaner for 30 minutes. Figure 2.4, shows the fabrication process of the OFET. The dielectric films were sandwiched between Al and Ag electrode to form a 2-mm^2 capacitor. 30-nm Al gate electrode was evaporated on the clean glass substrate by the vacuum evaporation method.

2.2.1. Poly(vinyl cinnamate) dielectric based OFET: 300 nm PVCN dielectric film was formed by spin-coating 40 mg/ml concentration of PVCN in chlorobenzene. Residual chlorobenzene solvent in the film was evaporated by annealing the film on a hot plate for 1 h after crosslinking it by UV (λ = 254 nm) treatment for 50 min. Source/drain Ag electrodes (50 nm) where deposited by vacuum evaporation method with a shadow mask defining the channel length and width to be 50 μm and 2 mm, respectively. In order to form a good interface with the semiconducting layer, the Ag source, drain electrodes where immersed in pentafluorobenzenethiol solution (0.005 mol/L) for 2 min. The electrodes were exhaustively rinsed with ethanol, then dried briefly on a hot plate. Spin-coating 10 mg/ml of Polystyrene (M_w = 600,000, Sigma Aldrich) and TIPS-pentacene (Ossila) with 3:1 ratio at1000 rpm formed the semiconducting layer. Furthermore, the film form was annealed for 30 min at 100 °C (all in dry nitrogen). The thickness of the semiconducting layer was measured to be 70 nm.

2.2.2. Biopolyamide dielectric based OFET: 40 mg/ml of the biopolyamide dissolved in dimethylformamide was spin-coated at 1000 rpm to form a dielectric layer of thickness 366 nm measured using a nanoscale hybrid microscope (VN-8000, Keyence). To complete the bottom-

gate bottom contact OFET device, the same experimental procedure was carried out as PVCN based OFET in 2.2.1 above. Figure 2.5 shows the device configuration of the biopolyamide and

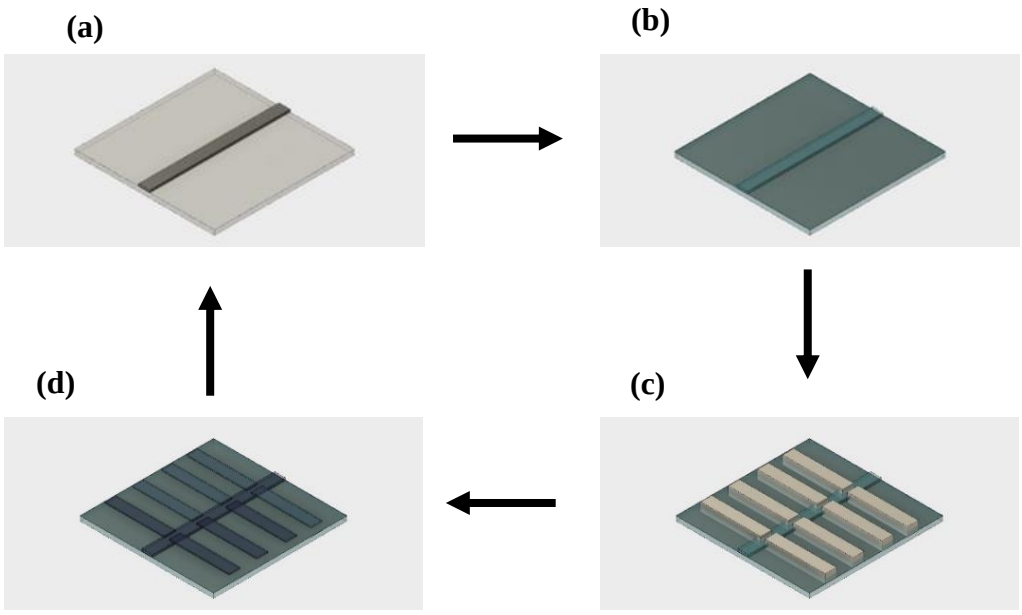

Figure 2.4. Schematic diagram of the fabrication procedure (a) 30 nm Al gate electrode on glass substrate; (b) dielectric layer on gate electrode; (c) Ag source-drain electrodes; (d) TIPS-pentacene/polystyrene semiconducting blend.

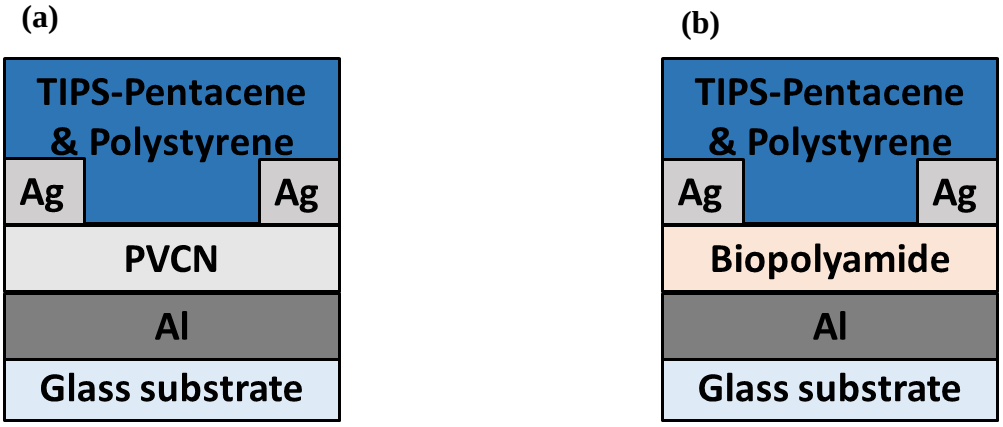

Figure 2.5. Bottom-gate bottom contact OFET with (a) PVCN as dielectric (b) biopolyamide as dielectric.

PVCN dielectric based OFET (see Figure 2.5 (a) and (b) respectively).

2.3. Results and Discussion

Here the results of the obtained from the characterization of PVCN and biopolyamide based OFET is discussed in section 2.3.1 and 2.3.2 respectively.

2.3.1. Characterization of Poly (vinyl cinnamate) dielectric for low voltage OFET

UV-vis characterization of the PVCN layer was used to check the photocrosslinking effect on the polymer; this is also known as (2+2) cycloaddition. Independent PVCN films were fabricated by spin-coating on an Al electrode/glass substrate, then inserted in a UV irradiation machine for different photochemical curing duration.

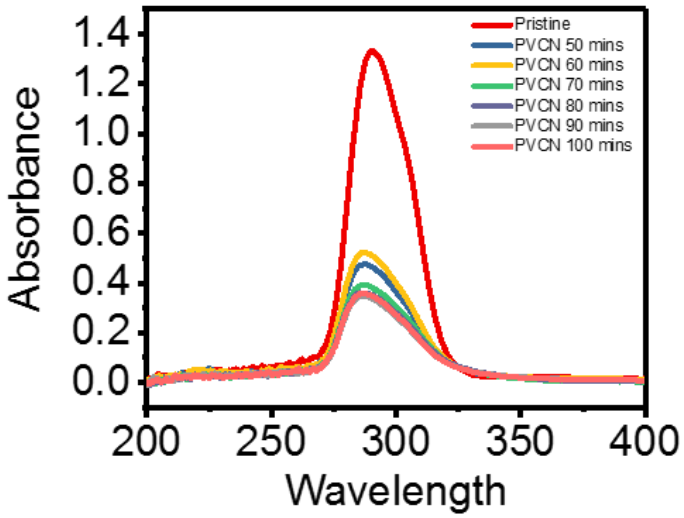

Figure 2.6. UV-vis crosslinking of PVCN before and after for time duration 50, 60, 70, 80, 90,100 minutes.

The C=C breaking of the aliphatic bonds in the cinnamate group led to decrease in the UV-vis absorbance peak seen in Fig.2.6. The wavelength in the range of 280 – 300 nm is consistent with

the C=C aliphatic bond [17, 18]. At a duration of 50 minutes, the crosslinking process is sufficient. To confirm the robustness of the PVCN film, current density-voltage characteristics using a metal insulator metal configuration seen in Fig. 2.7 below. The pristine PVCN current density is > 10^{-7}A at -5 V while the photocrosslinked PVCN film is as low as 10^{-11} A/cm^2. This implies that the

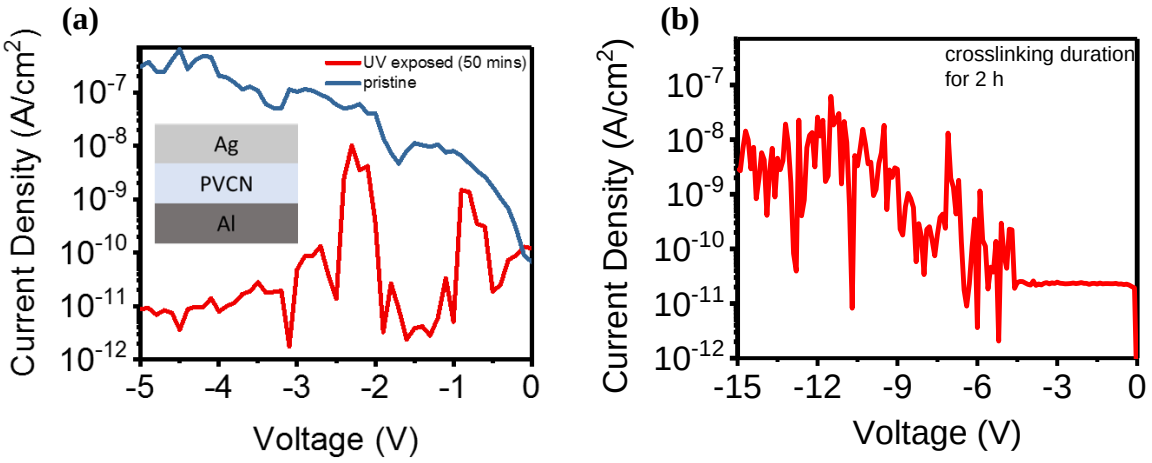

Figure 2.7. Current density-voltage electrical characterization of the PVCN film. (a) Pristine PVCN (in blue), (in red) (inset is the MIM device structure UV exposed PVCN film (50 mins) and (b) 2 h.

crosslinking of the polymer for 50 minutes was sufficient. However, increasing the crosslinking duration, increased the breakdown voltage of the PVCN dielectric film to 15 V with current density mostly less than 10^{-8} A/cm^2. The periodic change in the current density is possibly due to slow sweep voltage condition applied to the characterization system for measurement.

2.3.2. Characterization of biopolyamide dielectric for low voltage OFET

To investigate the resistance of the biopolyamide film to solution deposition of organic solvents, we spin coated chlorobenzene on it. We measured the surface morphology of the dielectric layer before and after this process using an atomic force microscope. Figure 2.8(a) and (b) shows the as-prepared biopolyamide film has a uniform morphology with root-mean-square of 0.1 nm and increased slightly to 0.6 nm when chlorobenzene was spin-coated on the dielectric layer. Thickness

of the film slightly reduced from 366 nm to 361 nm. It confirmed that the morphology of the biopolyamide was relatively unchanged when a commonly used organic solvent for OFET devices was deposited on it. The resistance to organic solvents makes the biopolyamide a suitable dielectric candidate for OFET devices other solution deposition methods. Using a contact angle meter

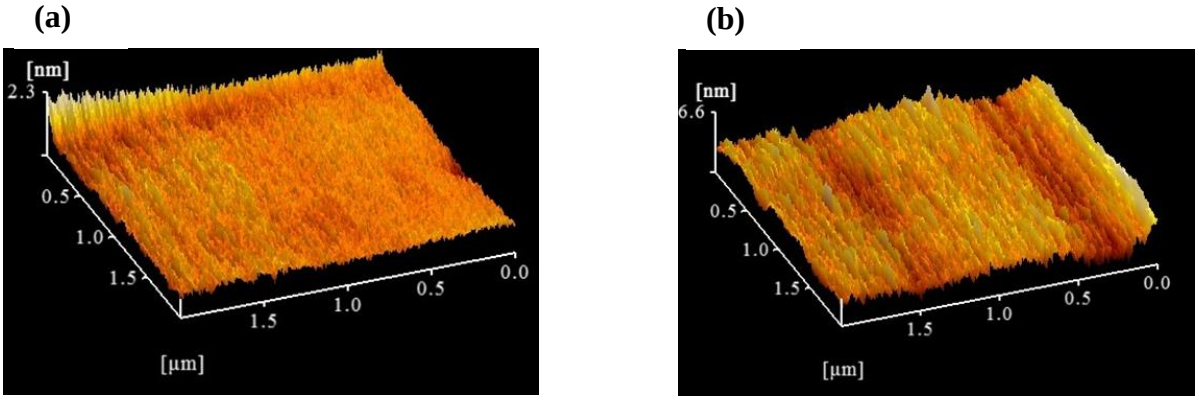

Fig. 2.8. AFM images of biopolyamide film cross-section before (a) and after (b) chlorobenzene spin-coating on it.

(Kyowa Interface Science Co. Ltd DMs-401) the water contact angle of the biopolyamide was measured to 59º. It also has a low surface energy of 44.7 mJ/m^2. The value of the surface energy is consistent with a hydrophobic hexamethyldisilazane (HMDS)-treated SiO_2 (43.6 mJ/m^2) and less than an untreated SiO_2 dielectric (61.4 mJ/m^2) [19]. Its surface energy is also similar to that of triacetate cellulose biopolymer [13] (41.3 mJ/m^2) therefore confirming the hydrophobic nature of the biopolyamide. The hydrophobic nature of the biomaterial showed that the material properties would not be affected by water vapor when exposed in the air. This makes the biopolyamide suitable for waterproof devices. To confirm the resistance of the biopolyamide to chlorobenzene solvent, the gate leakage current density and capacitance of the device were measured by sandwiching the biopolyamide dielectric in between Ag and Al electrodes to form a parallel plate capacitor. Figure 2.9(a) shows the current density against the voltage of the bio-based polyamide to be 10^{-11}A cm^{-2} at 5 V. Figure 2.9(b) shows the measured capacitance per unit area to be

independent of frequency in the frequency range: 10^2 Hz to 10^4 Hz. The relative constant capacitance value in this frequency range indicates that the polymer has few ionic impurities [7, 8]. The capacitance per unit area was extrapolated to be 12.25 nF cm^{-2} at 1000 Hz. Assuming a parallel plate capacitor, we calculated the dielectric constant of the biopolyamide to be 3.4.

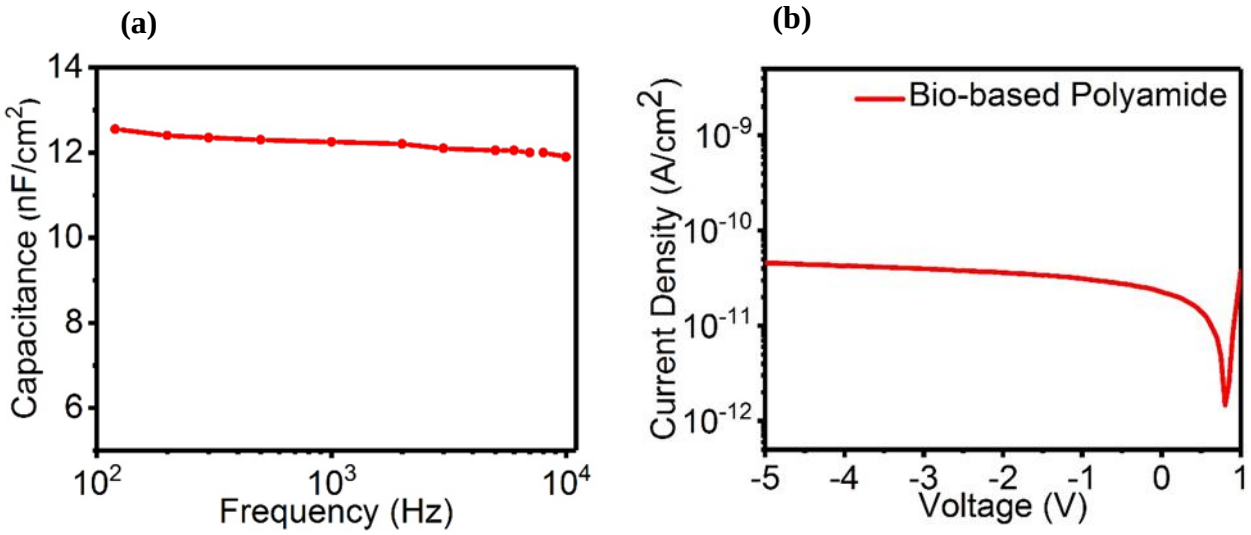

Figure 2.9. (a) Electric field leakage current density plot and (b) Frequency-dependent capacitance density for the biopolyamide film using the MIM device structure.

According to Veres *et al.* [7], low-k insulators were suggested to have a dielectric constant ranging from 2 to 18 by; therefore, this is a low-k dielectric material.

2.4. Basic Parameters of OFET

2.4.1. Poly (vinyl cinnamate)

Fig. 2.10(a) shows transfer characteristics of the low-voltage OFET by sweeping gate voltage, (V_G) from 1 V to – 5 V while keeping the drain voltage, (V_D) constant at -5 V. The field-effect mobility can be calculated from the saturation regime when $V_D > V_G$. The mobility, μ was calculated from drain current in the saturation regime equation:

$$I_{Dsat} = \frac{WC_i}{2L}\mu(V_G - V_{th})^2$$

Where W and L are the width and length of the channel 2 mm and 50 μm respectively. C_i is the capacitance of PVCN, 7.5 nF/cm^2. ON/OFF ratio of the device is 1.17 ×10^6; μ is the mobility of the device in the saturation region, 0.18 cm^2/Vs; V_{th} was deduced to be -0.15 V from the intercept of the root of drain current against V_G; In addition, the subthreshold swing, (SS), 125 mV/decade was deduced from the equation below:

$$SS = \frac{\partial \log I_D}{\partial V_G},$$

For the output characteristics, the drain current I_D was measured while V_D was varied at constant V_G. As seen in Figure 2.10(a) the low-voltage OFET exhibited typical p-type transfer characteristics with a linear increase in I_D at low V_D, then a saturation region is established by a constant V_D. The device showed negligible hysteresis because of the absence of hydroxyl ions in the PVCN material. The gate current was quite low 10^{-12} A, thus confirming that the photocrosslinked polymer withstood the electric field strength within the range of 1 V to -5 V gate voltage applied.

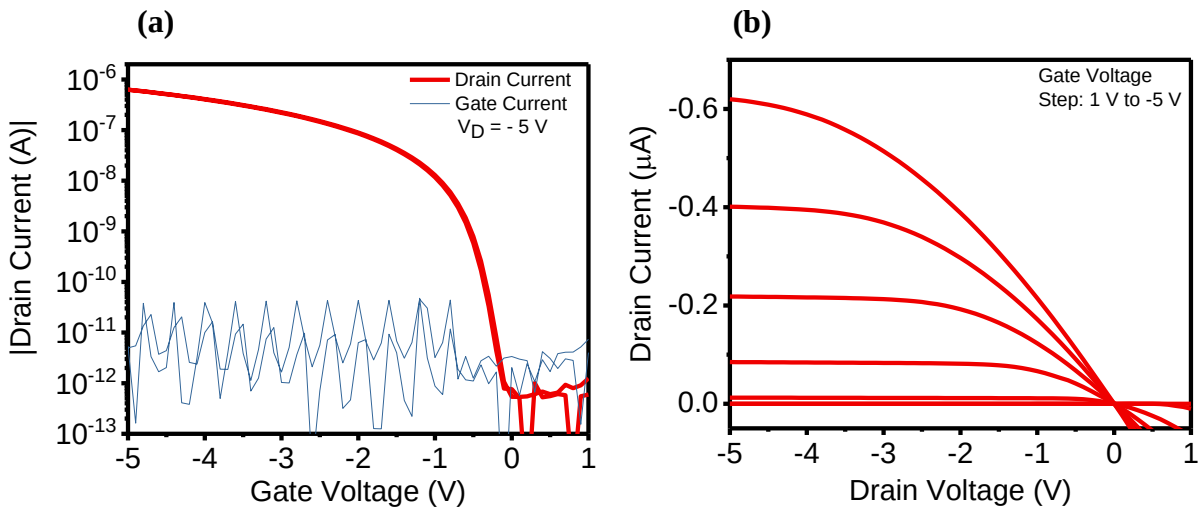

Figure 2.10. (a) Transfer and output (b) characteristics of PVCN based OFET

2.4.2 Biopolyamide based OFET

Figure 2.11(a) and (b) shows the transfer and output characteristics curve of the biopolyamide based OFET, respectively. Both show typical behavior of p-type OFETs with a drain current switching from linear to saturation region by scanning V_G from 1 V to -5 V at step 0.1 V. The negligible hysteresis observed may be due to the slow polarization effect and a few mobile ions or impurities in the film [7, 8]. The output and transfer characteristics show pinch-off current and saturation current curves. The device recorded a high on/off current ratio of 9.3×10^5, a low threshold voltage (V_{th}) of -0.85 V, and subthreshold swing (SS) of 108 mV/decade. The dielectric showed the great insulating property as the gate current, (I_G) recorded was about 3×10^{-11}A as seen in the transfer characteristics curve. The saturation field-effect mobility of the OFET is 0.27 cm^2/Vs. The high mobility is due to the crystallized semiconducting channel caused by the smooth surface of the biopolyamide. This is higher in comparison to other OFET based biopolymer dielectric materials, such as triacetate (0.031 cm^2/Vs) [13] and silk fibroin (0.21 cm^2/Vs) [20] in

which the semiconducting solutions were deposited via spin-coating. The OFET device was

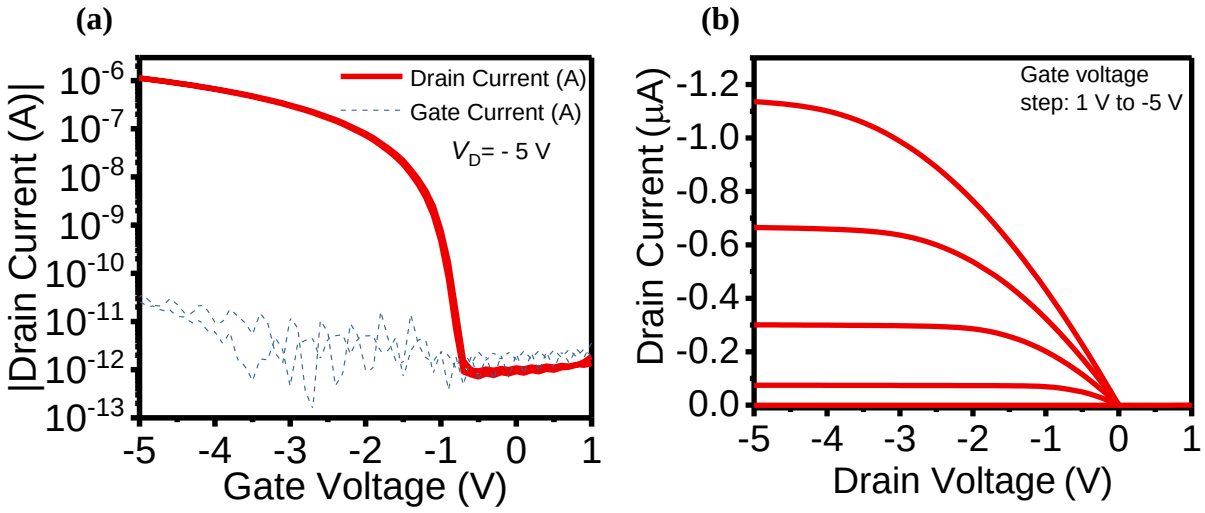

Figure 2.11. (a) Transfer and (b) output characteristics curves from the OFET devices with the biopolyamide as the dielectric.

fabricated with maximum processing temperature of 100 °C; and operation voltage of -5 V.

2.5. Conclusion

In summary, low-voltage OFETs using PVCN and a novel biopolyamide were fabricated and characterized. Both polymers showed significant resistance to chlorobenzene and formed good interface with a semiconducting blend of TIPS-pentacene and PS. The performance of the devices showed typical p-type transfer and output characteristics with negligible hysteresis, and low gate leakage current. The OFET devices were fabricated by solution-processing technologies, which are compatible to high-throughput printing of organic electronic devices in large areas.

References

[1] G. Gu, M. G. Kane, J. E. Doty, and A. H. Firester, Appl. Phys. Lett. **87**, (2015) 2435122005.

[2] H. E. Katz, X. M. Hong, and A. Dodabalapur, J. Appl. Phys. **91**, (2002) 1572.

[3] T. B. Singh, N. Marjanović, P. Stadler, M. Auinger, G. J. Matt, S. Gűnes,N. S. Sariciftci, R. Schwődiauer, and S. Bauer, J. Appl. Phys. **97**, (2005) 083714

[4] R. P. Ortiz, A. Facchetti, and T.J. Marks., Chem. Rev. **110**, (2010) 205-239

[5] J. Heo, S. Y. Parl, J. W. Kim, S. Song, Y. J. Yoon, J. Jeong, H. Jang, K. T. Lee, J. H. Seo, B. Walker, J.Y. Kim., Adv. Funct. Mater. **28,** (2018) 1704215.

[6] J. Veres, S.D. Ogier, S.W. Leeming, D.C. Cupertino and S.M. Khaffaf. Adv. Funct. Mater. **13,** (2003) 199-204

[7] S. C. Lim, S. H. Kim, J. B. Koo, J. H. Lee, C. H. Ku, Y. S. Yang, and T.Zyung, Appl. Phys. Lett. **89**, (2007) 173512

[8] S. Y. Yang, S. H. Kim, K. Shin, H. Jeon, and C. E. Park, Appl. Phys. Lett. **88**, (2006) 173507.

[9] J. Veres, S.D. Ogier and G. Lloyd Chem. Mater. **16**, (2004) 4543-4555.

[10] J. Jang, S. H. Kim, S. Nam, D.S. Chung, C. Yangm W. M. Yun, C.E. Park, J.B. Koo., **92**, (2008) 1433006

[11] J. Kang, N. Shin, D. Y. Jang, V. M. Prabhu, and D. Y. Yoon , J. Am. Chem. Soc. 2008, **30** (2008) 12273-12275.

[12] C.-H. Wang, C.-Y. Hsieh, J.-C. Hwang, C.-H. Wang, C.-Y. Hsieh, J.-C. Hwang, Adv. Mater. **23** (2011) 1630–1634.

[13] J.W. Bae, H.S. Jang, W.H. Park, S.Y. Kim, Org. Electron. **41** (2017) 186-189

[14] Y.S. Kim, K.H. Jung, U.R. Lee, K.H. Kim, M.H. Hoang, J. Il Jin, D.H. Choi, Appl. Phys. Lett. **96** (2010) 103307.

[15] J.W. Chang, C.G. Wang, C.Y. Huang, T. Da Tsai, T.F. Guo, T.C. Wen, Chicken albumen dielectrics in organic field-effect transistors, Adv. Mater. **23**(2011) 4077-4081

[16] S. Tateyama, S. Masuo, P. Suvannasara, Y. Oka, A. Miyazato, K. Yasaki, T. Teerawatananond, N. Muangsin, S. Zhou, Y. Kawasaki, L. Zhu, Z. Zhou, N. Takaya, T. Kaneko, Macromolecules. **49** (2016) 3336-3342.

[17] S. Furumi, K. Ichimura, H. Sata, and Y. Nishiura, Appl. Phys. Lett. **77,** (2000) 2689

[18] J.-H. Yoo, I. Cho, and S. Y. Kim, J. Polym. Sci., Part A: Polym. Chem. **42**, (2004) 5401.

[19] S.C. Lim, S.H. Kim, J.H. Lee, M.K. Kim, T. Zyung, Synth. Met. **148,** (2005) 75

[20] L. Shi, X. Xu, M. Ma, and L. Li. Appl. Phys. Lett. **104**, (2014) 023302

CHAPTER 3 || Dual-gate pressure sensor using P(VDF-TrFE) as top-gate dielectric*

In this chapter, a dual-gate organic pressure sensor composed of polarized P(VDF-TrFE) film and a low-voltage OFET allows measuring pressure in high ranges (> 100 kPa) is reported. When pressure is applied on the piezoelectric layer, the voltage generated modulates holes in the OFET's semiconducting channel, therefore, causing shift in threshold voltage (V_{th}). The pressure load applied varies linearly with V_{th} shift.

---

*O.O. Ogunleye, H. Sakai, Y. Ishii, H. Murata., Org. Electron., **75** (2019)

3.1. Introduction

Organic based piezoelectric materials show strong potential for applications in touch sensing devices for future robotic applications. One of such material is PVDF (poly vinylidene fluoride) which exists in various phases: α, β, γ and δ. These phases are classified based on the orientation of the hydrogen and fluorine molecules with respect to the centre of the polymer chain. With the co-polymer TrFE, β phase P(VDF-TrFE) can easily be achieved by solution-processing methods. Figure 3.1. shows a schematic representation of α and β phases of P(VDF-TrFE) films respectively. Piezoelectricity cannot be achieved when P(VDF-TrFE) films are in α phase because of the random orientation of dipoles leading to a net cancellation. For surface charges to be generated, the dipoles need to align parallel to each other into a β phase structure. This phase orientation could be achieved by electrical poling or stretching.

Figure 3.1. Schematic structure of (a) α and (b) β phase P(VDF-TrFE) films

This organic material has been explored for both piezoelectric and pyroelectric sensing applications [2, 3]. In addition, its ferroelectric property has made it suitable for memory devices [4]. Its copolymer P(VDF-TrFE) (poly(vinylidene fluoride trifluoroethylene)) show a higher piezoelectric property compared to PVDF and are ferroelectric when deposited by solution process [5, 6]. When annealed at 140 °C, the polymer is crystallized and the β phase orientation of the polymer is automatically formed without mechanical stretching. The ratio of the VDF to TrFE molecules plays a strong role in the β phase formation of the dipoles. The molar mass of the TrFE

molecules is between 15 to 40 % of the P(VDF-TrFE) total molar mass [3]. The solid film, mesoporous, film or nanofiber forms of the material has been used as sensing layer in nanogenerators and pressure sensors [7-12].

The orientation of the CF_2 molecules of this polymer depends on annealing temperature ranging from 130 °C to 160 °C. When polarized by an electric field, the direction of the net dipole moment of the polymer is oriented perpendicular to the substrate and in the same direction of the electric field. Therefore, applying pressure parallel to the polarization direction induces the generation of charges on its surface; this is due to the strain exerted on the piezoelectric material.

Since the crystal structure of P(VDF-TrFE) is orthorhombic, it has a crystal symmetry of C_{2v} [14]. This implies that the matrix form of its piezoelectric tensor, d_{ij} is reduced to five independent non-zero piezoelectric coefficients, as shown below:

$$d_{ij} = \begin{pmatrix} 0 & 0 & 0 & 0 & d_{15} & 0 \\ 0 & 0 & 0 & d_{24} & 0 & 0 \\ d_{31} & d_{32} & d_{33} & 0 & 0 & 0 \end{pmatrix}$$

Here, d_{ij} is the piezoelectric tensor with i as the electric field direction and j as stress/pressure direction. Figure 3.2 shows the schematic diagram of the P(VDF-TrFE) film where direction 3 is normal to the film. The direction of polarization is also depicted to be downward.

This research focuses on d_{33} because the direction of stress and the direction of the electric field is normal to the surface of the piezoelectric film as well as the direction of polarization. Using electric fields greater than 1 MV/cm for the poling procedure, an enhanced d_{33} of 47 pC/N was achieved; however, the device fabrication process is expensive and not compatible with the high-

throughput fabrication process. In addition, the operation voltage of the TFT was 15 V, which is not reliable for wearable devices [15]. Using crystalline silicon MOS with high mobility of up to 85 cm^2/V.s, and a polarized 2.5 μm thick P(VDF-TrFE) layer spin-coated on the gate, a piezoelectric oxide field effect transistor pressure sensor was fabricated [16].

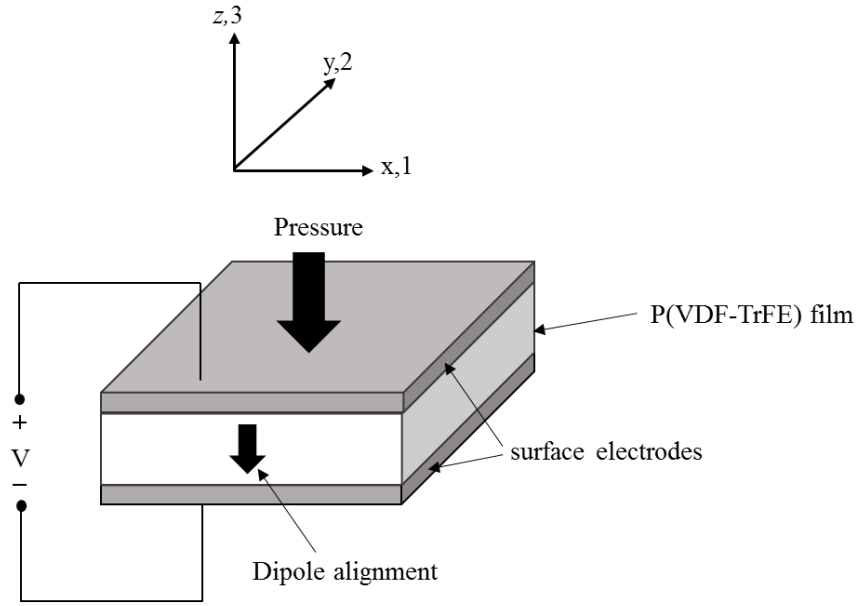

Fig. 3.2. Schematic diagram of the P(VDF-TrFE) film showing the directions 1, 2, and 3 representing the drawn, transverse and thickness directions respectively.

This device has enormous applications for touch sensing because of its excellent measurement of dynamic normal forces [17]; however, it is not compatible with a non-planar surface such as the human skin.

In this chapter, the fabrication process and characterization of an organic pressure sensor with -5 V operation voltage is discussed [13]. The sensing layer used is a polarized P(VDF-TrFE) with low-voltage OFET as the read-out element. The sensor measured pressure between 113 kPa-451 kPa. A linear relation between the threshold voltage and pressure was obtained, therefore showing the reliability of the device. Unlike crystalline silicon MOS and TFT, solution processes were used

to deposit the device active layers, which is compatible with roll-to-roll manufacturing of these pressure sensors. A proposed operation mechanism for the low voltage dual-gate organic transistor based pressure sensor was discussed based on the direction of polarization, the interaction of bound charges of the P(VDF-TrFE) with the mobile charge carriers accumulated in the semiconducting channel of the organic transistor.

3.2. Experimental Methods

To fabricate the dual-gate OFET pressure sensor, first, a low-voltage OFET was fabricated. The glass substrate was cleaned in acetone for 5 min, then in IPA for 10 min. The glass substrates surface were further cleaned to remove any residual contaminants using a UV ozone cleaner for 30 min.

300 nm PVCN dielectric film was formed by spin-coating 40 mg/ml concentration of PVCN in chlorobenzene. Residual chlorobenzene solvent in the film was evaporated by annealing the film on a hot plate for 1 h after crosslinking it by UV (λ = 254 nm) treatment for 50 min. Source/drain Ag electrodes (50 nm) where deposited by vacuum evaporation method with a shadow mask defining the channel length and width to be 50 μm and 2 mm, respectively. In order to form a good interface between the Ag source, drain electrodes where immersed in pentafluorobenzenethiol solution (0.005 mol/L) for 2 min. The electrodes were exhaustively rinsed with ethanol, then dried briefly on a hot plate. Spin-coating 10 mg/ml of Polystyrene (M_w = 600,000, Sigma Aldrich) and TIPS-pentacene (Ossila) with 3:1 ratio at1000 rpm formed the semiconducting layer. Furthermore, the film form was annealed for 30 min at 100 °C (all in dry nitrogen). The thickness of the semiconducting layer was measured to be 70 nm.

The sensing layer was fabricated by blade coating P(VDF-TrFE) solution (0.15 g/ml) in N-methyl-2-pyrrolidinone solvent 3 times on a Si wafer, then heating the film for 1 h at 140 °C to crystallize the film. 75:25 is the molar ratio of VDF to TrFE (Kureha Corp.). To improve the piezoelectric property of the crystallized 12 μm-thick polymer film the film was polarized with a poling voltage of -1000 V by forming a capacitor which included the bladed coated Si/P(VDF-TrFE) film with a Si substrate placed on the film. The contact poling process was carried out by

grounding the top Si electrode while applying a poling voltage on the other Si electrode. The resistivity of the Si substrates ranges from 0.1-100 Ωcm. To complete the dual-gate gate organic pressure sensor, the P(VDF-TrFE) layer was superimposed on the active layer of the low-voltage OFET with the piezoelectric layer facing the active layer of the OFET. Independently fabricating the OFET and P(VDF-TrFE) sensing layer prevents orthogonality problem arising from the N-methyl-2-pyrrolidinone solvent and the TIPS-pentacene/polystyrene semiconducting layer of the OFET. A quasistatic piezoelectric measurement system (see Fig. 3.3) was used to measure piezoelectric constant of the P(VDF-TrFE) films [18]. A charge amplifier was used to measure electric charges that flowed between the probe and Si substrate when an 8.0 mm diameter disk-shaped metallic probe was loaded periodically on the films. This procedure occurred in an interval of approximately 2.9 s with the periodically applied load and preload to be 6.0 N and 4.0 N, respectively. To get d_{33}, the produced charge by the film was divided by the given difference of the loads (2.0 N).

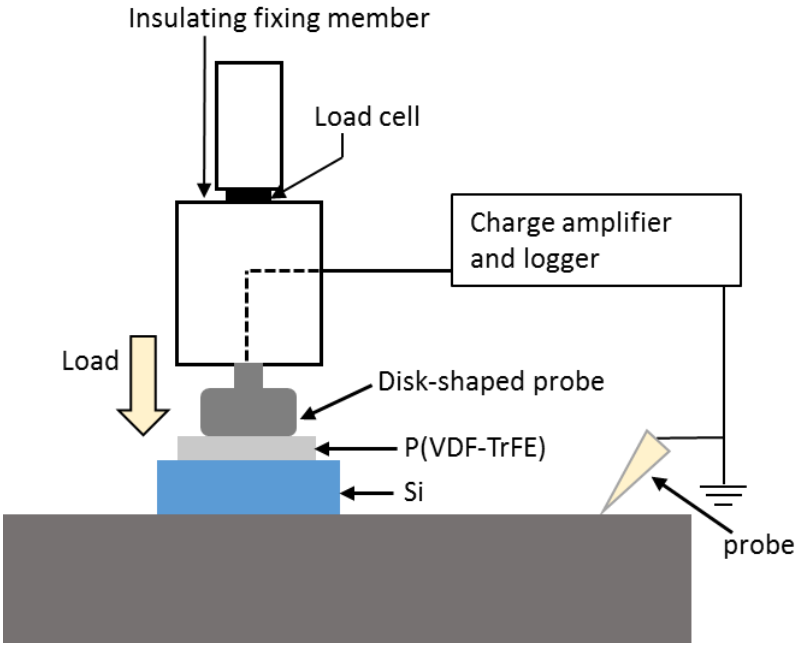

Figure 3.3. Schematic diagram of the contact poling process

3.2.1. Blade Coating process

Blade coating process was used to make the P(VDF-TrFE) films. 0.15 g/ml concentration of P(VDF-TrFE) solution in N-methyl-2-pyrrolidinone was stirred on a hot plate overnight. The solution was then blade coated on a silicon substrate using a mask. Figure 3.4 shows a picture of the blade coating process with the solution deposited onto the silicon substrate. The blade coated film was placed on a hot plate at 140 °C for 3 minutes to evaporate. The same blade coating process was repeated 2 times consecutively. After the third time, the films were annealed for hours to crystallize the P(VDF-TrFE) films. The thickness of the film measured was 12 μm. Figure 3.4 shows a schematic diagram of the contact poling process used to polarize the P(VDF-TrFE) layer.

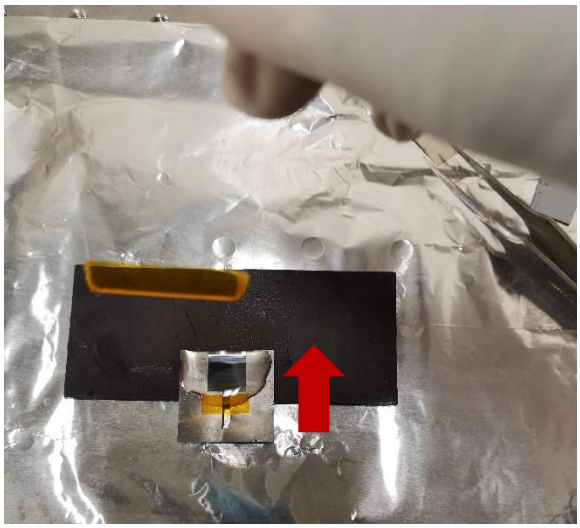

Figure 3.4. Picture showing of blade coating process: Al mask placed on the Si substrate attached to a magnet and solution deposited on the Si substrate.

Figure 3.5 shows a schematic diagram of the contact poling process utilized to polarize the films. In Fig. 3.5(a), the PVDF-TrFE film was blade coated on a Si substrate. It was then crystallized by annealing the film at 140 °C for 1 h. The films were polarized by contact poling at room temperature conditions. To carry out the poling process, the crytallized film was sandwiched between bottom silicon electrode and a top Si electrode (see Fig. 3.5(b)). The top Si electrode was grounded while a d.c. poling voltage of -1000 V was applied to the bottom Si electrode for at least

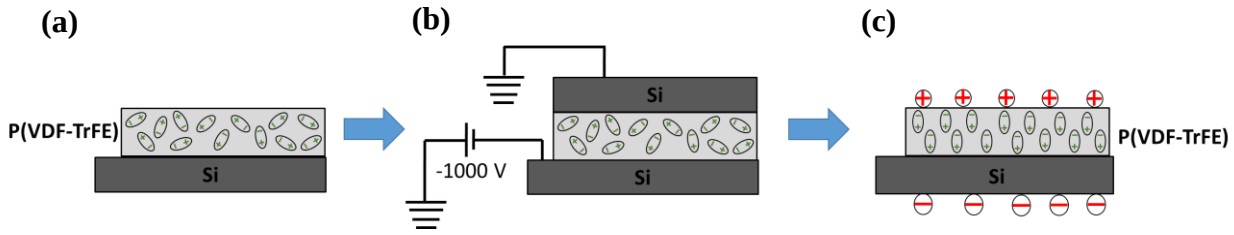

Figure 3.5. Schematic diagram of the contact poling process

45 min. Fig. 3.5 (c) shows the the top-Si electrode removed from the polarized P(VDF-TrFE) film leaving the film polarized. To check the the polarity of the surface potential induced by polarizing the P(VDF-TrFE) film, the film was placed not more than 10 mm away from a digital low voltage static meter seen in Fig. 3.5. The static sensor detector is to the right of the main unit unit which records the static voltage on the surface of the film. Therefore, surface potential of the P(VDF-TrFE) film was confirmed to be positive using a Digital Low Static Meter (MODEL KSD-3000) seen in Fig. 3.6.

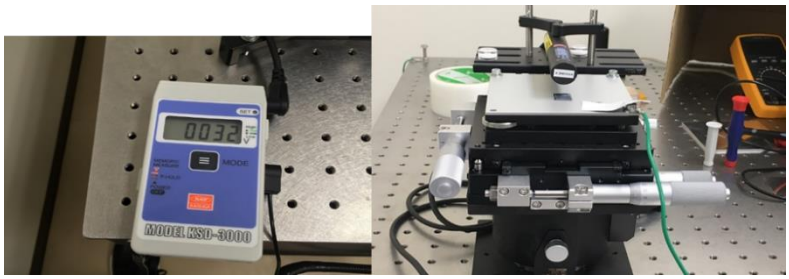

Figure 3.6. Digital low voltage static meter showing positive surface potential value of the polarized P(VDF-TrFE) film.

3.3. Results and Discussion

The bottom-gate OFET was first electrically characterized. The typical transfer characteristics of the bottom-gate OFET is shown in Fig. 3.7(a). The gate voltage (V_G) was swept from 1 to -5 V in steps of 0.1 V at a constant drain voltage (V_D) of -5 V. The output characteristics of the OFET is shown in Fig. 3.7(b). V_G was scanned from 1 to -5 V in steps of -1 V while the V_D was swept from 1 to -5 V in steps of 0.1 V. The field-effect mobility, on/off ratio, subthreshold swing (*SS*) and V_{th}, value were extracted to be 0.8 cm^2/Vs, 1.1×10^6, 115 mV/decade and 0.18 V respectively.

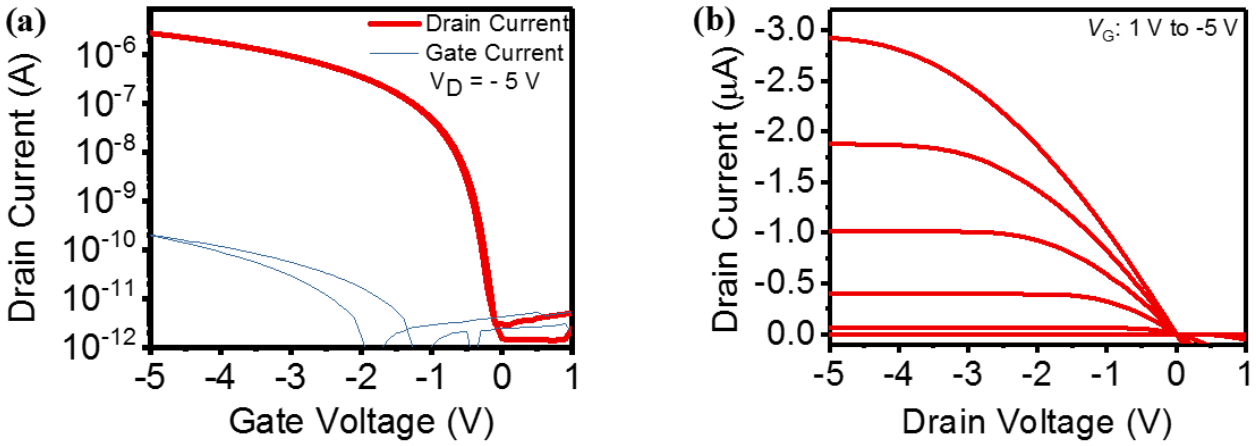

Fig. 3.7. OFET (a) transfer (b) Output characteristics

These results agree that the device operated at a low-voltage and is consistent with low-voltage OFET devices using TIPS-pentacene/polystyrene film as the semiconducting layer and PVCN as dielectric [13]. Figure 3.8(a) shows a schematic diagram of a polarized P(VDF-TrFE) layer stacked on the bottom-gate OFET. Figure 3.8(b) shows the polarized P(VDF-TrFE) layer placed on the active layer of the fabricated low voltage OFET and the gate, drain voltage of the OFET were applied. The surface potential of the TIPS-pentacene layer is changed by the surface charges on the piezoelectric film.

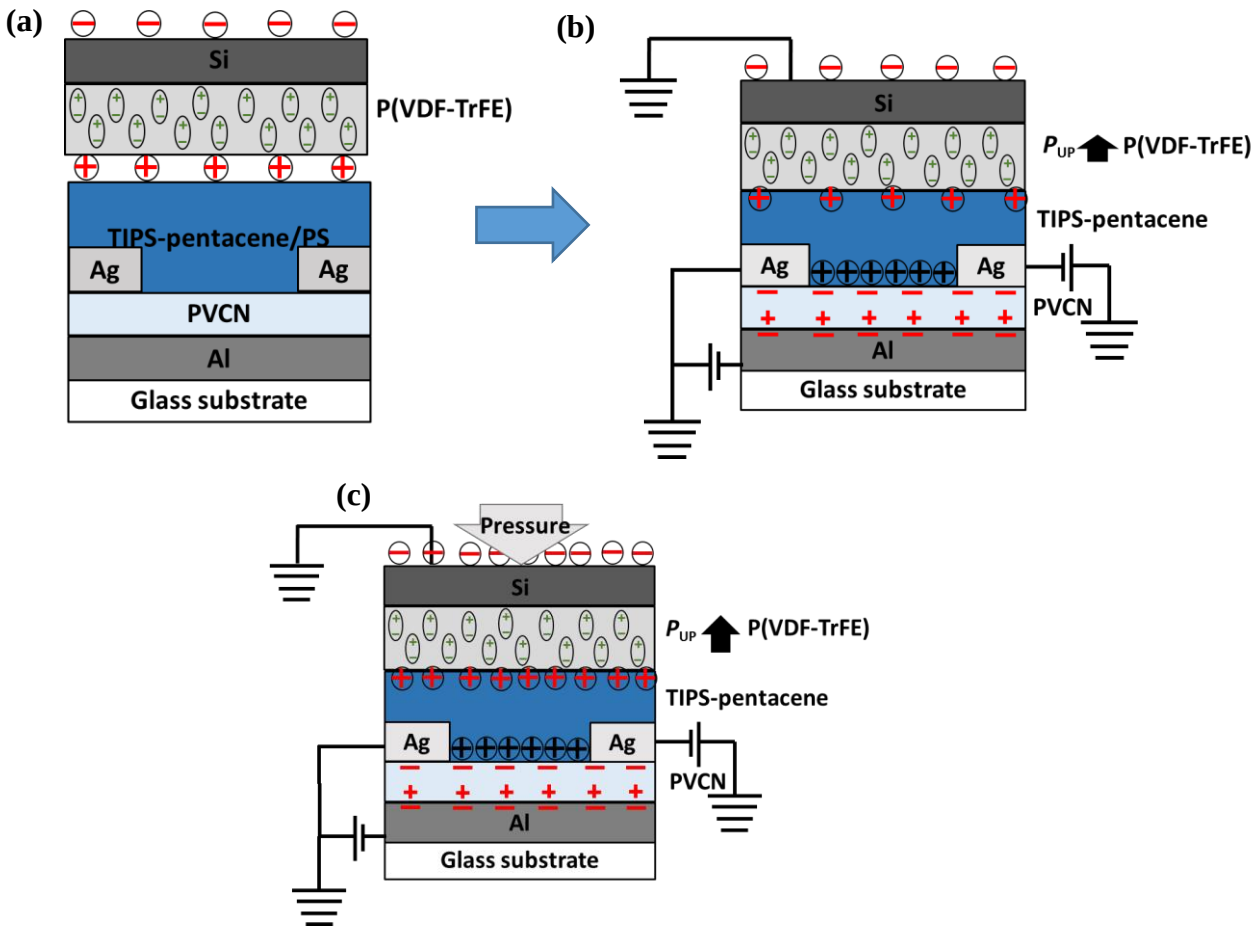

Figure 3.8. Schematic diagram of the (a) P(VDF-TrFE) film above the low-voltage OFET dual-gate pressure sensor (b) P(VDF-TrFE) film placed on the low-voltage OFET (c) pressure load exerted on the P(VDF-TrFE) film.

This led to a shift in the transfer curve, therefore confirming the polarization of the P(VDF-TrFE) film. This shift agrees with a previous study indicating that the P(VDF-TrFE) layer is polarized [13], therefore, the surface potential on the polarized P(VDF-TrFE) film and the TIPS-pentance/polystyrene layer induces the initial shift in V_{th} when in contact. Figure 3.8 (c) shows the surface charges at the interface of the piezoelectric and semiconducting layer. When pressure is exerted on the piezoelectric film, the polarization of the film is changed producing electric field. Furthermore, the magnitude of the electric field depends on pressure exerted on the piezoelectric

film. The pressure load on the piezoelectric layer gives rise to a shift in transfer characteristics which depends on the magnitude of the pressure load as seen in Fig. 3.9(c). This caused the production of surface charges at the region of the piezoelectric and semiconducting layer causing an electric field which opposes the gate field. This caused the depletion of mobile charge carriers accumulated in the channel of the OFET (in black, see Fig. 3.8(c)). To compensate for mobile charge carriers depleted, the gate voltage increases because more mobile charge carriers have to be injected to create the semiconducting channel. The correlation between the initial shift of the transfer curve and the magnitude of the surface potential of the P(VDF-TrFE) layer was described in chapter 6. The transfer characteristics at different pressure loads on the device is shown in Fig 3.9(b). I_D-V_G sweeps were carried out at each pressure value. Pyroelectric effect was mitigated because measurements were carried out at room temperature. During measurements, the top-gate Si electrode was grounded. The pressure load was increased from 113 kPa to 451 kPa leading to transfer curve shifts which returned to the original position when the pressure load was removed showing that this device operated as a pressure sensor. Figure 3.9 (c) shows relationship between V_{th} shift and pressure load is linear. The amount of charges, Q the piezoelectric film produces is approximately proportional to the force applied, F, with d_{33} as the piezoelectric constant [15, 16, 19]. However, when a positive voltage is used to polarize the P(VDF-TrFE) film, the induced screening charges in the surface of the semiconducting layer are negative (see Fig. 3.10 (a)). The electric field interaction between the negative screening charges and the mobile charge carriers leads to an accumulation of charge carriers in channel, therefore a shift to the right of the transfer curve is observed in Fig. 3.11.

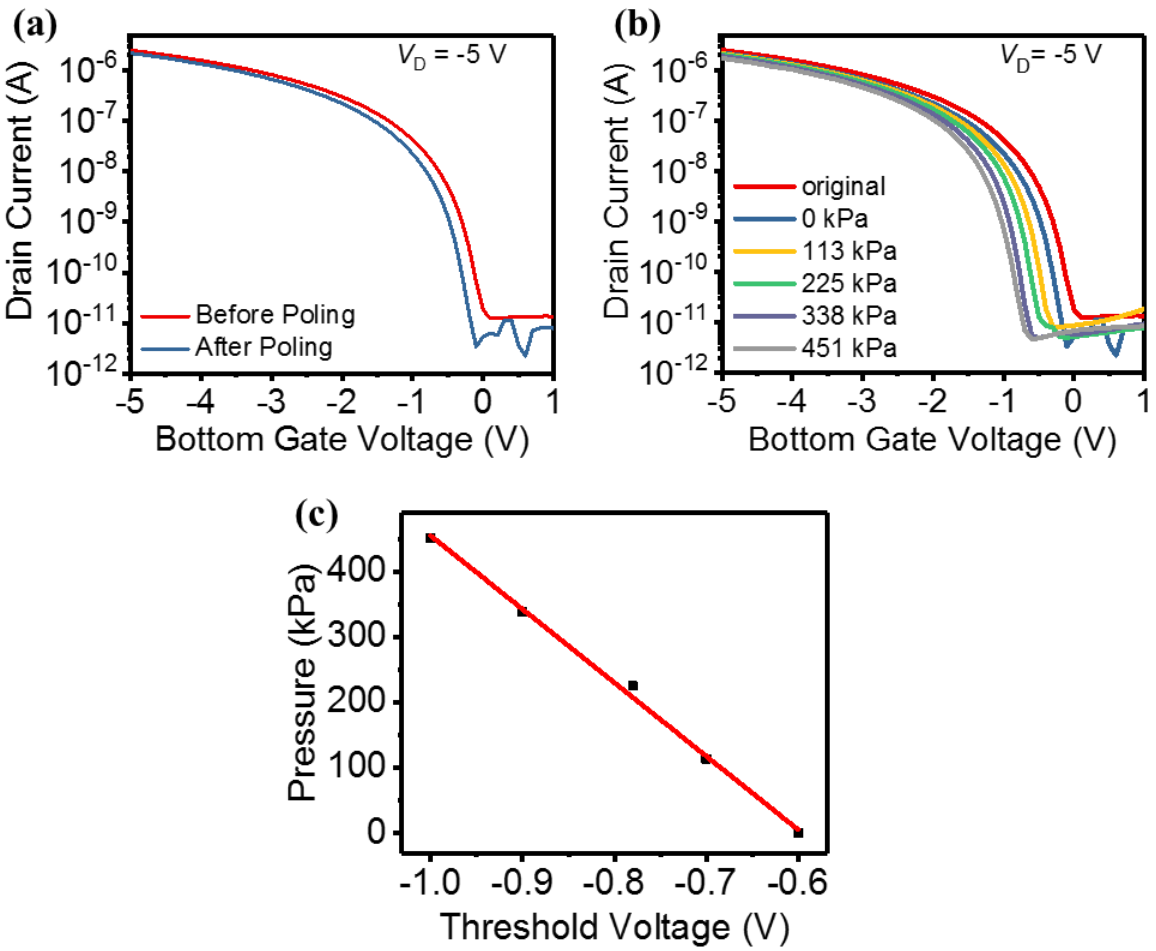

Fig. 3.9. (a) Threshold shift when polarized P(VDF-TrFE) was placed on the active layer. (b) Transfer curve shifts corresponding to pressure load. (c) linear relation between pressure load and threshold voltage.

This may be due to the enhancement of the gate field by the electric field between the mobile charge carriers and the screening charge. When 100 kPa pressure load is placed on the P(VDF-TrFE) film the device is ON at 0 V gate potential due to the enhanced electric field caused by negative screened charges formed on the piezoelectric film [20] (see Fig. 3.11).

.

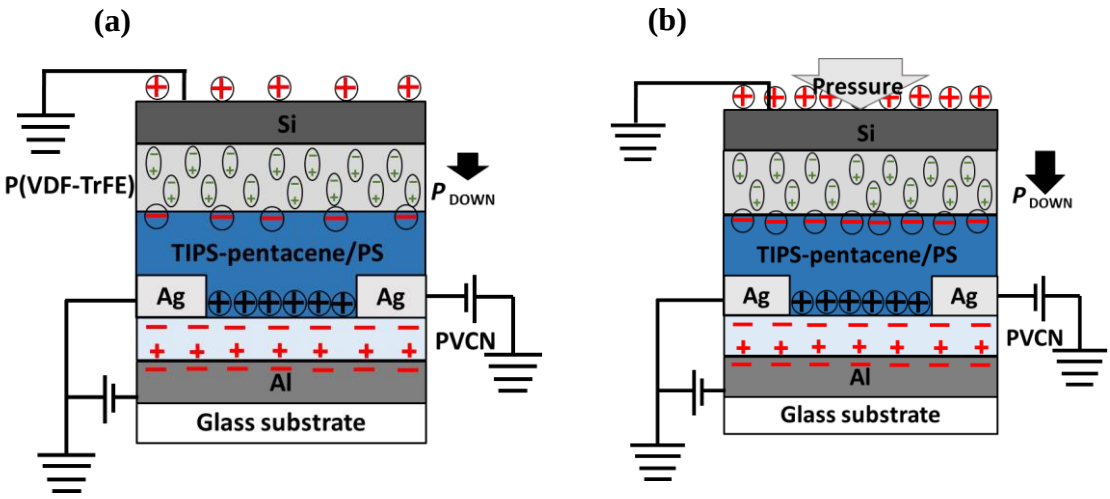

Figure 3.10. Schematic diagram of (a) P(VDF-TrFE) film placed on the low-voltage OFET (b) pressure load exerted on the P(VDF-TrFE) film.

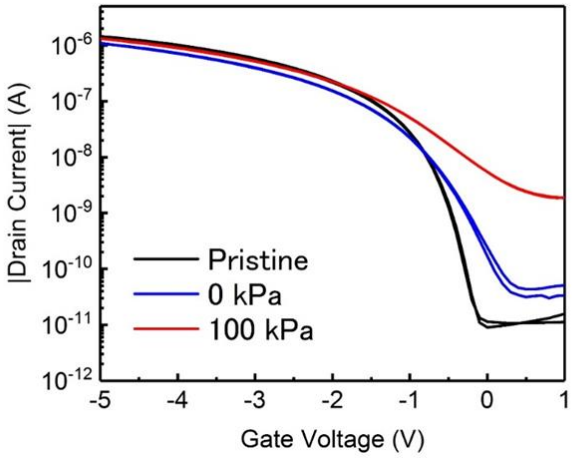

Fig. 3.11. Transfer curve shift when P(VDF-TrFE) film is positively poled

Exerting pressure load on the piezoelectric film displaces fixed charges in the piezoelectric film, causing an increase in the induced charges at the region of the semiconducting layer and P(VDF-TrFE) film (see Fig. 3.10(b)).This phenomenon agrees with the conventional operation mechanism of dual-gate OFET in which applying a positive voltage to the top gate electrode reduces the number of charge carriers or holes collected at the drain electrode of the bottom-gate OFET [21]. However, applying a negative top-gate voltage leads to more charge carriers collected in the drain electrode of the bottom-gate OFET.

3.4. Conclusion

In summary, an organic pressure sensor consisting of a polarized P(VDF-TrFE) film and low-voltage OFET was successfully fabricated and characterized. The polarized P(VDF-TrFE) film acted as a top-gate sensing voltage induced by a pressure load causing V_{th} shift in the transfer characteristics curve. This V_{th} shift is linear to the pressure load, thus confirming the successful operation of the pressure sensor. A proposed sensing mechanism to describe the interface interaction between the bound charges produced by the polarized P(VDF-TrFE) material and the semiconducting layer was discussed.

References

[1] T. Sharma, S-S. Je, B. Gill, J.X.J. Zhang. Sensors and Actuators A **177** (2012) 87-92

[2] R.S. Dahiya, G. Metta, M. Valle, A. Adami, and L. Lorenzelli. Applied Physics Letters, **95** (2009) 034105

[3] S. Hannah, A. Davidson, I. Glesk, D. Uttamchandani, R. Dahiya, H. Gleskova. Org. Electron. **56** (2018) 170-177

[4] R. C. G. Naber, C. Tanase, P.W.M. Blom, G. H. Gelinck, A. W. Marsman,, F. J. Touwslager, S. Setayesh & D. M. De Leeuw, Nature Materials, **4** (2005), 243-248.

[5] A. Laudari, A.R. Mazza, A. Daykin, S. Khara, K. Ghosh, F. Cummings, T. Muller, P.F. Miceli, and S. Guha, Physical Review Applied, **10** (2018) 014011

[6] A.J. Lovinger J. Macromolecules, **18** (1985) 910-918

[7] G. Ren, F. Cai, B. Li, J. Zheng & C. Xu. Macromolecular Materials and Engineering, **298** (2013) 541-546.

[8] K. Takashima, S. Horie, T. Mukai, K. Ishida, K. Matsushige. Sensors and Actuators A: Physical, **144** (2008) 90-96.

[9] X. Li and E.C. Kan. Sensors and Actuators A: Physical, **163** (2010) 457-463.

[10] J-H. Lee, H-J. Yoon, T. Y. Kim, M.K. Gupta, J. H. Lee, W. Seung, H. Ryu, S-W. Kim, Adv. Mater. **25** (2015) 3203-3209

[11] Z. Pi, J. Zhang, C. Wen, Z-B. Zhang, D. Wu. Adv. Mater. **7** (2014) 33-41.

[12] A. Aliane, M. Benwadih, B. Bouthinon, R. Coppard, F-D. Santos, &, A. Daami. Organic Electronics, **25** (2015) 92-98.

[13] Y. Tsuji, H. Sakai, L. Feng, X. Guo, and H. Murata. Applied Physics Express **10** (2017) 021601.

[14] G. M. Sessler, Electrets-volume 1, The Laplacian press series, California, 1998.

[15] F. Maita, L. Maiolo, A. Minotti, A. Pecora, D. Ricci, G. Metta, G. Scandurra, G. Giusi, C. Ciofi, and G. Fortunato. IEEE Sensors Journal. **15** (2015) 3819-3826

[16] R.S. Dahiya, G. Metta, M. Valle, IEEE Trans. Ultrason., Ferroelectr., Freq. Control. **56** (2009) 2.

[17] A. Spanu, L. Pinna, F. Viola, L. Seminara, M. Valle, A. Bonfiglio, P. Cosseddu., Org. Electron., **36** (2016), 57-60.

[18] Y. Ishii, S. Kurihara, R. Kitayama, H. Sakai, Y. Nakabayashi, T. Nobeshima, S. Uemura. Smart Mater. Struct., 28 (2019) 08LT02.

[19] ANSI/IEEE, IEEE standard on piezoelectricity. IEEE Standard 176-1987 (1987).

[20] T. Ishikawa, H. Sakai, H. Murata. IEICE TRANS. ELECTRON., **E102–C** (2018) 188-191.

[21] J. J. Brondijk, M. Spijkman, F. Torricelli, P. W. M. Blom, and D. M. de Leeuw1, Appl. Phys. Lett. **100** (2012) 023308.

CHAPTER 4 || Low-voltage Dual-gate OFET using CYTOP as top-gate dielectric

In this chapter, dual-gate OFETs device using CYTOP as top-gate dielectric and PVCN as bottom-gate dielectric were fabricated and characterized. The on/off ratio and mobility remained approximately the same, despite shift in the threshold voltage. The bias top-gate voltage controlled the threshold voltage of the bottom gate potential. A linear relation was established between the top-gate voltage and the threshold voltage. The top-gate induced electrostatic potential led to a depletion of holes accumulated at the dielectric/semiconductor interface causing threshold shift.

4.1. Introduction

Organic materials are solution-processable, therefore easily used to manufacture large-area, low-cost, transparent, lightweight and flexible devices [1-3]. One of such device is the organic field effect transistor (OFET) which has been used as read-out elements for sensing applications [4-6]. However, they are most unstable when exposed to the atmosphere, thus must be encapsulated when used in ambient air. The electrical performance of the device also degrades with time. One such electrical parameter that changes over time due to the instability of the organic semiconducting layer is the threshold voltage (V_{th}). According to Spijkman et al., V_{th} defines the gate voltage at which the depletion current is lowest, and the accumulation current is highest [7]. Thus, V_{th} defines the sensitivity of sensors, the noise margin in logic devices as well as the performance of an OFET device [8, 9]. To achieve high sensitivity in sensor devices, V_{th} has to be controlled to obtain maximum results. Also, for electronic logic circuits, the V_{th} has to be controlled to maximize the noise margin.

Various methods have been studied on controlling V_{th} of OFETs which include self-assembled monolayers (SAM) [10]. The drawback, in the end, the SAM may destroy or change the chemistry of the organic layers of the device, yielding to unreliable results. Another method tried has been the use of passivation layers to shield the organic layers from the air, therefore protecting the device. This may not be efficient on an industrial scale because of the extra costs required to carry out this process.

This has led to the dual-gate OFET device (see Fig. 4.1), in which electrostatic potential from the top-gate (or bottom gate) voltage depletes, or modulated charge carriers accumulated in the bottom (or top) channel of the device [11-13]. These charge carriers in the bottom channel are induced by the gate potential applied to the bottom gate of the device. The concentration of charge carriers

depleted in channel corresponds to the electrostatic potential generated by the gate voltage, therefore leading to controllable V_{th} shift without destroying the organic layers.

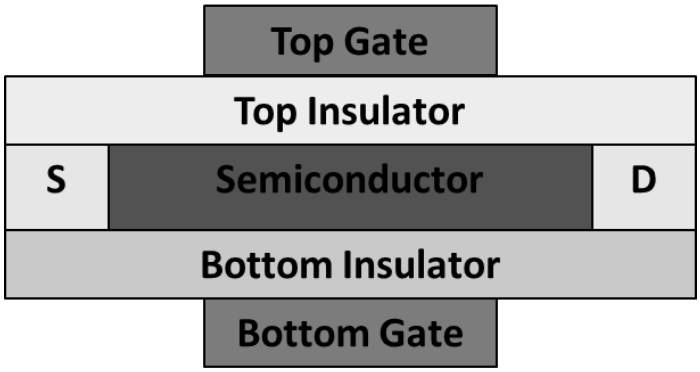

Fig. 4.1. Schematic structure of the dual-gate OFET

The total charge (Q_{total}) induced by both gates is given by equation (1) [7]:

$$Q_{\text{total}} = C_{\text{bottom}}V_{\text{bottom}} + C_{\text{top}}V_{\text{top}} \quad \ldots\ldots\ldots\ldots\ldots\ldots\ldots (1)$$

Where C_{top} the capacitance of the top-gate dielectric, while C_{bottom} is the capacitance of the bottom-gate dielectric. The total charge at the threshold voltage, V_{th} is zero, therefore, equation (1) becomes $C_{\text{bottom}}V_{\text{bottom}} = -C_{\text{top}}V_{\text{top}}$. For a p-type semiconducting layer, with a negative bias bottom-gate voltage, with a fixed top-gate voltage, the threshold voltage, V_{th} could be deduced from the equation (2) shown below [7]:

$$V_{\text{th}} = -\frac{C_{\text{top}}}{C_{\text{bottom}}}V_{\text{TG}} \quad \ldots\ldots\ldots\ldots\ldots\ldots\ldots\ldots\ldots (2)$$

In this chapter, a dual-gate OFET with top and bottom gate dielectric, PVCN and CYTOP were fabricated and characterized. The results of the device showed a controllable V_{th} shift of the bottom-gate potential when a biased V_{TG} was applied. CYTOP solution was used because TIPS-pentacene is easily dissolvable by most organic solvents [14].

4.2. Experimental methods

The device structure of the dual-gate OFET can be seen in Fig. 4.2. A low voltage OFET device was fabricated on a glass substrate. The glass substrate was cleaned for 5 minutes using Acetone and then using IPA for 10 minutes, all in an ultrasonic bath. The glass substrates were then dried using a spin-coating machine. Then further dried on a hot plate at 100 °C for 3 min. 30 nm thick Al gate electrodes were vacuum evaporated on the glass substrates.

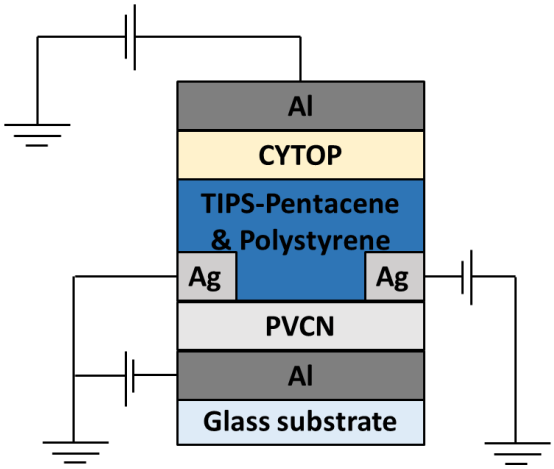

Fig 4.2. Device configuration of a dual-gate OFET

300 nm PVCN dielectric film was formed by spin-coating 40 mg/ml concentration of PVCN in chlorobenzene. Residual chlorobenzene solvent in the film was evaporated by annealing the film on a hot plate for 1 h after crosslinking it by UV ($\lambda = 254$ nm) treatment for 50 min. Source/drain Ag electrodes (50 nm) where deposited by vacuum evaporation method with a shadow mask defining the channel length and width to be 50 μm and 2 mm, respectively. In order to form a good interface with the semiconducting layer, the Ag source, drain electrodes where immersed in pentafluorobenzenethiol solution (0.005 mol/L) for 2 min. The electrodes were exhaustively rinsed with ethanol, then dried briefly on a hot plate. Spin-coating 10 mg/ml of Polystyrene (M_w = 600,000, Sigma Aldrich) and TIPS-pentacene (Ossila) with 3:1 ratio at1000 rpm formed the

semiconducting layer. Furthermore, the film form was annealed for 30 min at 100 °C (all in dry nitrogen). The thickness of the semiconducting layer was measured to be 70 nm. The dual-gate OFET device was completed by depositing a 950 nm-thick top gate dielectric layer by spin-coating CYTOP (CTL-809M) at 2000 rpm on the semiconducting film. The Cytop dielectric film was dried on a hot plate at 100 °C for 20 min.

4.3. Basic Parameters of dual-gate OFET

Figure 4.3(a) and (b) show the transfer and output characteristics of the dual-gate OFET when the top-gate voltage, V_{TG} is grounded. The transfer characteristics of the low-voltage OFET was measured by sweeping the gate voltage, (V_G) from 1 V to – 5 V while keeping the drain voltage, (V_D) constant at -5 V. The field-effect mobility can be calculated from the saturation regime when $V_D > V_G$. The mobility, μ was calculated from drain current in the saturation regime equation:

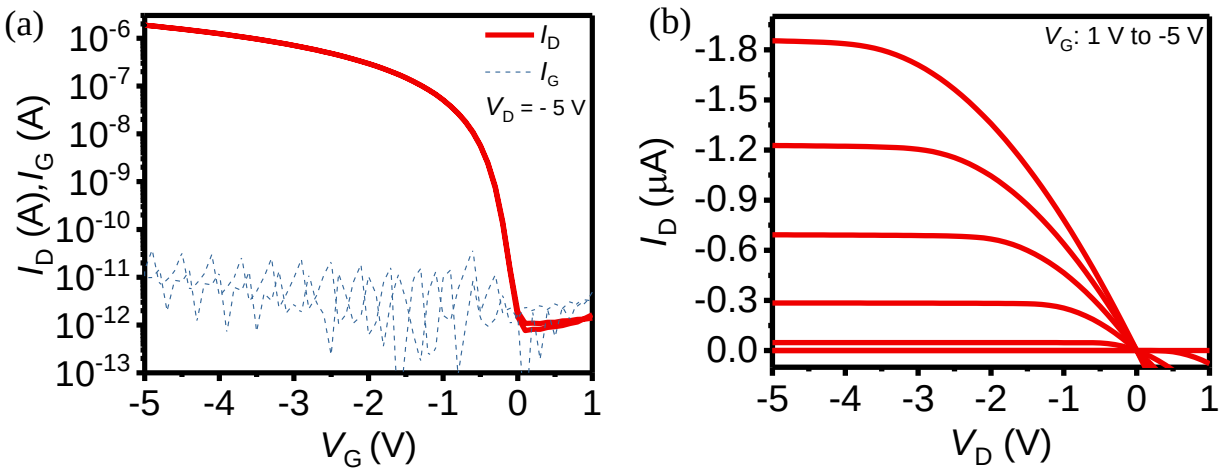

Figure 4.3. (a) Transfer and (b) output characteristics of the dual-gate OFET with V_{TG} grounded.

$$I_{\mathrm{Dsat}} = \frac{WC_i}{2L}\mu(V_{\mathrm{G}} - V_{\mathrm{th}})^2,$$

Where W and L is the width and length of the channel respectively. The width of the channel is 2 mm while its length is 50 μm. C_i is the capacitance of PVCN, 7.5 nF/cm^2. ON/OFF ratio of the device is 1.13 ×10^6, μ is the mobility of the device in the saturation region, 0.48 cm^2/Vs; V_{th} was deduced to be 0.12 V from the intercept of $(I_D)^{0.5}$ against V_G; In addition, the subthreshold swing, (SS), 110 mV/Dec was deduced from the equation below:

$$SS = \frac{\partial \log I_D}{\partial V_G},$$

For the output characteristics in Fig. 4.3(b), the drain current I_D was measured while V_D was varied at constant V_G. As seen in Fig. 4.3(a) the low-voltage OFET exhibited typical p-type characteristics with a linear increase in I_D at low V_D, as well as saturation region with the increase in V_D.

4.4. Mechanism Discussion

When bottom-gate voltage, V_{BG} is swept from 1 V to -5 V, charge carriers are accumulated at the bottom channel of the OFET. At V_{TG} = 0, the top-gate electrode is grounded, the device performance is similar to a bottom-contact bottom gate OFET. When a positive top-gate voltage is applied, a controllable V_{th} shift is observed at constant V_D of -5 V, as seen in Fig. 4.4(a) and (b).

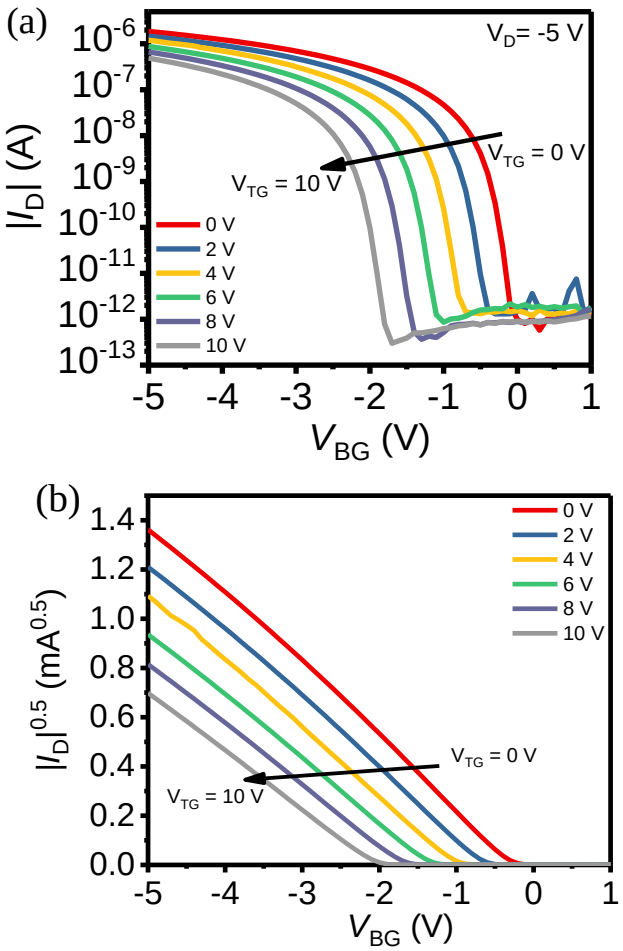

Figure 4.4. (a) V_{th} controllable transfer curves of transistors (b) square root of drain current curves as a function V_{BG}.

The ON/OFF ratio remains 10^6 notwithstanding the change of V_{TG}. V_{th} is extracted from $|I_D|^{0.5}$ against V_{BG} curves shown in 4.4. (b); the μ remains the same regardless of the change in $|I_D|^{0.5}$ caused by the change in V_{TG}. Fig. 4.5 shows an in increase V_{TG} corresponding to a linear increase in V_{th}.

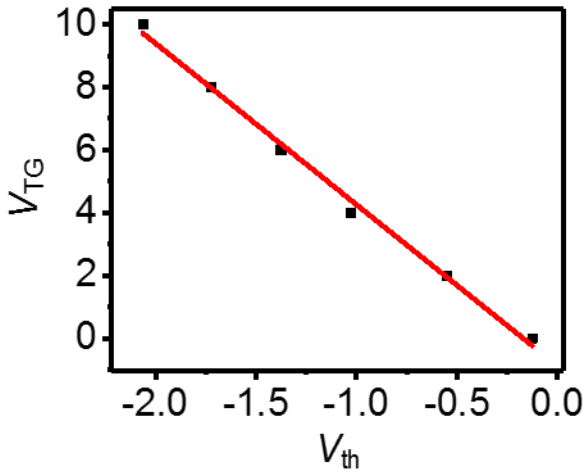

Figure 4.5. Graph of V_{TG} against V_{th}.

The values of V_{th} are -0.125 V and -2.0625 V with V_{TG} values 0 V and 10 V respectively. The controllable increase of V_{th} is approximately 0.4 V. From parallel-plate capacitor, the capacitance of Cytop is calculated to be 1.9 nF/cm^2 given the relative permittivity of Cytop to be 2.0 and thickness of 950-nm. The capacitance of PVCN bottom dielectric layer is 7.5 nF/cm^2. Substituting the capacitance of Cytop and PVCN in equation (2) the V_{th} shift is approximately 0.5 V given V_{TG} to be 2 V. The estimated V_{th} shift is slightly consistent with V_{th} shift obtained experimentally by change in V_{TG}.

Since there are no electrons induced at the CYTOP/TIPS-pentacene interface (p-type semiconducting channel), the charge carriers in the bottom channel are not shielded from the electrostatic potential. Applying voltage to the top-gate electrode, V_{TG} caused the charge carrier depletion in the channel, which establishes a shift in V_{th}. Increasing V_{TG} leads to a corresponding

increase in the electrostatic potential, which implies that more charge carriers in the channel are depleted. Hence, a similar V_{th} shift is observed as seen in Fig. 4.4 (a). This is consistent with results of a dual-gate OFET [11-13]. In addition, the CYTOP layer encapsulates the device, therefore protecting the device from ambient air and possible degradation [15].

4.5. Conclusion

In summary, a dual-gate OFET was successfully fabricated and characterized. The V_{th} from the bottom gate potential was controlled by biasing the V_{TG}. The relation between the V_{th} and V_{TG} is linear, agreeing with the results reported for dual-gate OFETs. V_{th} of the low-voltage bottom OFET was controlled perfectly. This research may be useful to low-voltage OFETs with unreliable V_{th} values due to instability of their organic layers.

References

[1] M. Berggren, D. Nilsson, and N. D. Robinson, Nat. Mater. , **6** (2007) 3–5

[2] A. C. Arias, J. D. MacKenzie, I. McCulloch, J. Rivnay, and A. Salleo, Chem. Rev. **110** (2010) 3–24

[3] G. H. Gelinck, *et al.* Nat. Mater. **3** (2004) 106–110.

[4] S. Lai, P. Cosseddu, A. Bonfiglio and M. Barbaro, IEEE Electron Device Letters, **34** (2013) 801-803.

[5] G. Schwartz, B.C.-K. Tee, J. Mei, A.L. Appleton, D.H. Kim, H. Wang, Z. Bao, Nat. Commun. **4** (2013) 1-8

[6] A. Chortos, J. Liu and Z. Bao. Nat. Mater. **15** (2016) 937-950.

[7] M.-J. Spijkman, K. Myny, E. C. P. Smits, P. Heremans, P. W. M. Blom, D. M. de Leeuw, Adv. Mater. **23** (2011) 3231-3242

[8] M.-J Spijkman, E. C. P. Smits, P. W. M. Blom, D. M. de Leeuw, Y. Bon Saint Come, S. Setayesh, E. Cantatore, Appl. Phys. Lett. **92** (2008) 143304

[9] Y. Tsuji, H. Sakai, L. Feng, X. Guo and H. Murata. Applied Physics Express **10** (2017) 021601

[10] N. Stutzmann, R. H. Friend, H. Sirrighaus, Science **299** (2003) 1881.

[11] F. Maddalena, M. Spijkman, J. J. Brondijk, P. Fonteijn, F. Brouwer, J. C. Hummelen, D. M. de Leeuw, P. W. M. Blom, B. de Boer, Org. Electron. **9** (2008) 839-846

[12] S. Iba, T. Sekitani, Y. Kato, T. Someya, H. Kawaguchi, M. Takamiya, T. Sakurai, S. Takagi, Appl. Phys. Lett. **87** (2005) 023509

[13] J. J. Brondijk, M. Spijkman, F. Torricelli, P. W. M. Blom, and D. M. de Leeuw1, Appl. Phys. Lett. **100** (2012) 023308.

[14] A. M. Gaikwad, Y. Khan, A. E. Ostfeld, S. Abraham, A. C. Arias Org. Electron. **30** (2016) 18-29

[15] W. Tang, L. Feng, P. Yu, J. Zhao, and X. Guo. Adv. Electron. Mater., **2** (2016) 1500454

CHAPTER 5: SENSING MECHANISM OF THE LOW-VOLTAGE DUAL-GATE PRESSURE SENSOR*

Dual-gate organic pressure sensors consist of piezoelectric P(VDF-TrFE) sensor in combination with a low-voltage OFET as read-out element. The depletion of charge carriers in the channel of the OFET was caused by pressure-induced voltage from the piezoelectric layer leading to a shift in V_{th} depletes charge carriers accumulated in the channel of the OFET, causing a shift in threshold voltage. Results obtained from both the dual-gate pressure sensor and a conventional dual-gate OFET, showed that the piezoelectric constant of the sensing layer to be 72 pC/N. This value is in the same order with the piezoelectric constant of the film measured directly confirming that the dual-gate pressure sensor operation mechanism was caused by piezoelectric behavior of the P(VDF-TrFE) layer used in the device.

*O.O. Ogunleye, H. Sakai, Y. Ishii, H. Murata., Org. Electron, **75** (2019).

5.1. Introduction

In order to use OFETs operating with low voltages for pressure sensors, charge carriers accumulated in the semiconducting channel could be controlled by signal output from pressure load. Conventional dual-gate OFETs demonstrate that a top-gate voltage could modulate mobile charge carrier accumulated in the channel of a bottom-gate OFET [1, 2]. Sandwiched between the top and bottom gate electrodes is the organic semiconducting layers as well as equivalent organic insulating layers. By biasing the bottom gate with a specific voltage, accumulated charges are induced at dielectric/semiconductor interface. When top gate is applied, charge carriers accumulated in the channel are depleted causing a change in V_{th}.

Polarized P(VDF-TrFE) material produces charges or voltages in response to pressure load placed on them [3, 4]. The dipoles aligned parallel in the film produces surface charges when force is placed on it. The charge carriers induced the semiconducting channel of the OFET are modulated by the surface charges which is similar to the functionality of a top-gate voltage in a dual-gate OFET [5].

Recently, the piezoelectric property displayed by P(VDF-TrFE) inspired the development of a low-voltage dual-gate OFET based pressure sensor, with low operation voltage of -5 V. The configuration of the novel device was made up of a piezoelectric P(VDF-TrFE) film laminated on the active layer of the OFET [6]. A significant $\Delta I/I_o$ of 155 was achieved when pressure load of 300 kPa was exerted on it. The dual-gate OFET based pressure sensor makes use of the piezoelectric dielectric layer as the top gate insulator, which eventually generates this top-gate bias voltage when pressure exerted on it. This is similar to the operation of a dual-gate OFET of which top-gate applied caused a shift in the transfer curve. Previously, a qualitative operation mechanism

of the dual-gate OFET based pressure sensor was suggested but a quantitative clarification was lacking.

In this chapter, dual-gate organic pressure sensor operation mechanism was investigated. The operation of the dual-gate OFET based pressure sensor was shown to be caused by the piezoelectric behavior of the polarized P(VDF-TrFE) sensing layer. Charge carriers in the channel of the OFET were controlled by the sensing layer which agrees with the performance of the OFET used for pressure sensing. Also, the shift in V_{th} as well as shift in transfer characteristics is consistent with that of a dual gate organic pressure sensor. The amount of holes depleted in the channel of the OFET could then be estimated by pressure exerted on the piezoelectric layer. In addition, d_{33} (72 pC/N) of the sensing layer was obtained from results of both devices. This agreed with the value (53 pC/N) obtained when d_{33} of the sensing layer was directly measured.

5.2. Quantitative Analysis

To unveil the dual-gate OFET based pressure sensor operation mechanism, d_{33} of P(VDF-TrFE) layer in the dual-gate OFET based pressure sensor was estimated from correlation between the applied pressure and V_{th} shift. The V_{th} shift was caused by a change in the sensing voltage as a function of the applied pressure, giving rise to the possibility that V_{th} shift is caused by piezoelectric effect. If this were to be the case, the d_{33} value of the P(VDF-TrFE) calculated based on pressure response of the pressure sensor would agree with d_{33} value of P(VDF-TrFE) film measured. Equation (1) below was used to estimate d_{33} of P(VDF-TrFE) layer in the dual-gate OFET based pressure sensor: the quantity of charges (Q) generated by the piezoelectric sensing layer is proportional to force applied (F), with d_{33} as the piezoelectric constant of P(VDF-TrFE) [7, 8].

$$Q = d_{33} F \ldots \ldots \ldots (1)$$

Taking into consideration the relation between F and Q, equation (1) is rearranged to give equation (2):

$$Q/A = d_{33} F/A \ldots \ldots \ldots (2)$$

Where F/A is simply pressure exerted on the sensor. The pressure load required to obtain per unit amount of change in the V_{th} shift is the slope described as $F/A \times V_{th}^{-1}$ and extrapolated to be c.a. 11.2×10^5 Pa/V from Fig. 5.1(b). When pressure is applied to the piezoelectric sensing layer, (Q/A) produced by the piezoelectric sensing layer is accumulated at the P(VDF-TrFE)/TIPS-pentacene interface layer. As shown in Fig. 5.1 (a), these charges may have caused the V_{th} shift, which is equivalent to the top-gate voltage (V_{Top}) applied on the conventional dual-gate OFET. A

conventional dual-gate OFET was fabricated and characterized to estimate *Q/A* generated by the piezoelectric layer.

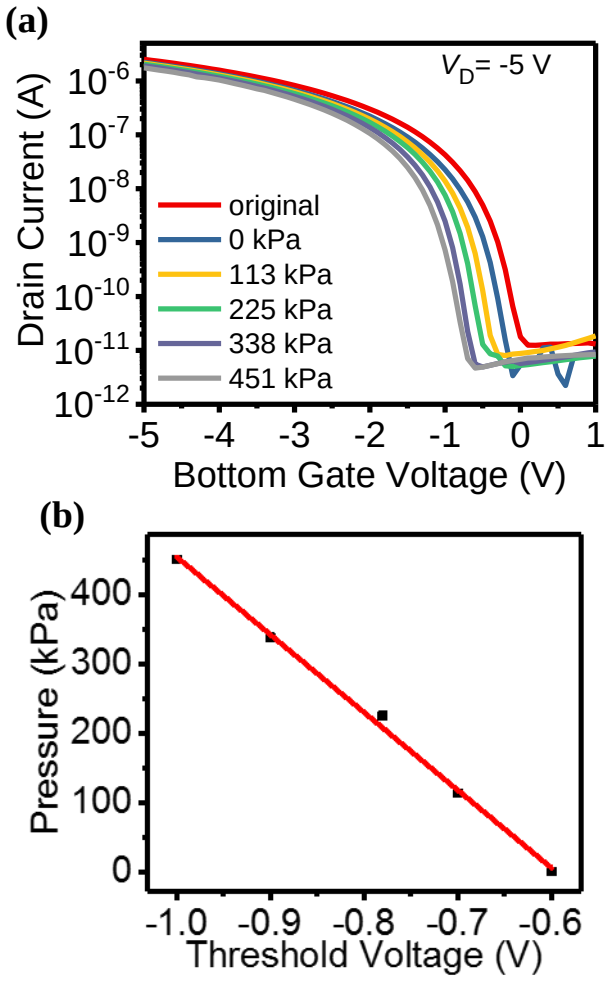

Figure 5.1 (a) Transfer curve shifts corresponding to pressure load (b) graph of pressure load against threshold voltage

The top-gate dielectric layer of the conventional dual-gate OFET differs from that of the dual-gate organic pressure sensor. However, the bottom-gate OFET used for both devices are similar as well as the operation voltage applied. Therefore, the quantity of *Q/A* that leads to the V_{th} shift of the OFET is considered to be consistent. The transfer curves of the conventional dual-gate OFET. Is shown in Fig. 5.2(a). The transfer curve shifts in line with the magnitude of V_{Top}. The depletion of

charges in the OFET channel is caused by the electrostatic potential changes which is not shielded by the semiconducting layer [9].

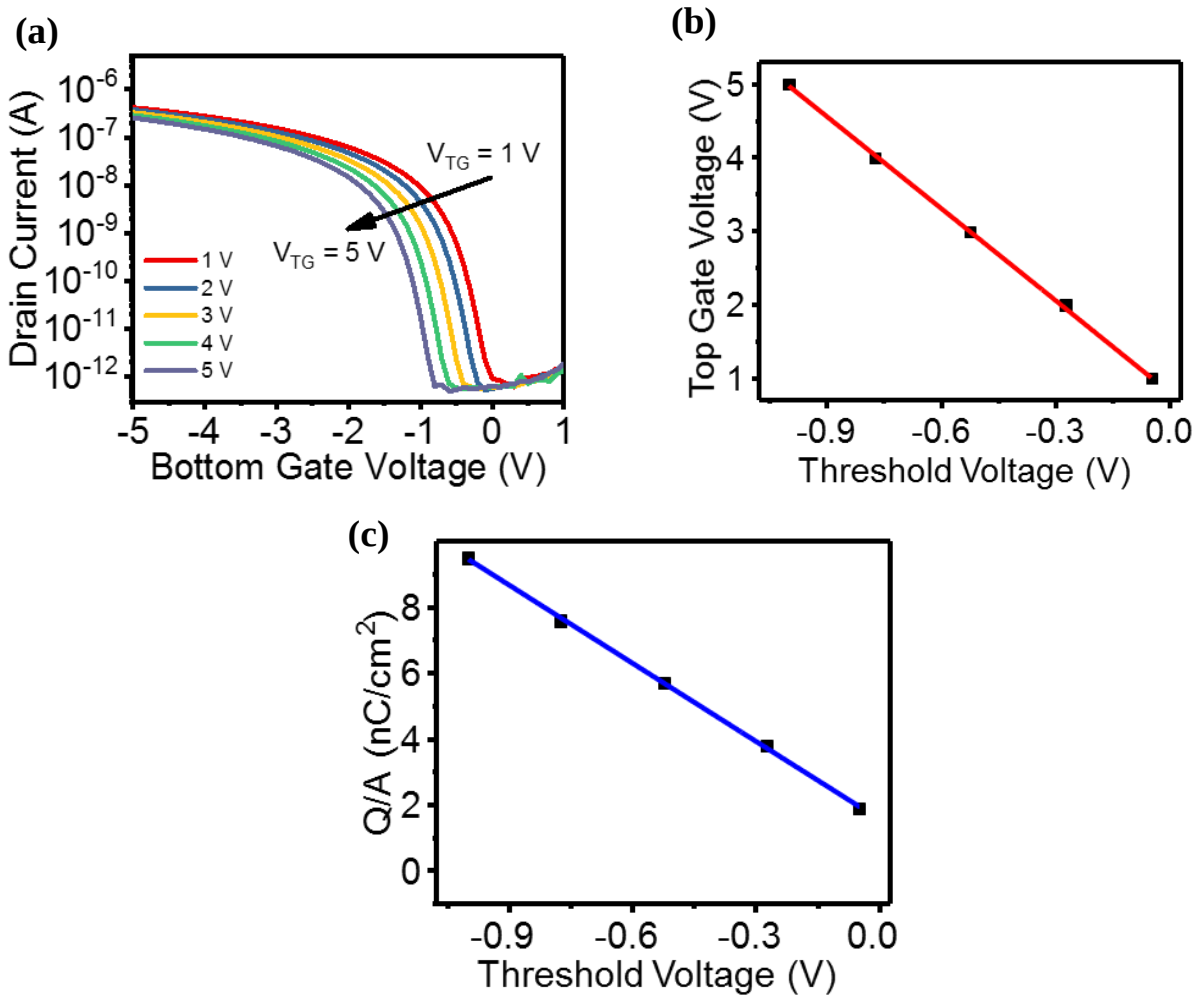

Fig. 5.2. (a) Threshold shift of the OFET corresponding to top-gate voltage (b) graph of Top gate voltage against threshold voltage (c) graph of threshold voltage against charge per unit area.

Fig. 5.2 (b) shows that the relationship between the V_{Top} and V_{th} is linear. This shift in V_{th} was caused by positive V_{Top} which is typical of a dual-gate OFET. *Q/A* accumulated at the interface between the TIPS-pentacene semiconducting layer and top-gate dielectric (Cytop) V_{Top} was estimated from the equation (3) [2].

$$Q/A = C_T V_{Top} \ldots \ldots \ldots (3)$$

Where C_T (1.9 nF/cm^2) capacitance of the Cytop layer and A is the unit area of the CYTOP layer. From this calculation, the relation between V_{th} and V_{Top} can be replotted as the relation between Q/A and V_{Top} (Fig. 5.2(c)). The value of Q/A to obtain per unit amount of change in the V_{th} shift can be described as $Q/A \times V_{th}^{-1}$, which is the slope of Fig. 4(c) and calculated to be 8.1 nC/cm^{2}V. Here, the F/A and Q/A quantitative correlation in equation (2) with respect to unit change in V_{th} shift is achieved. Furthermore, by inserting the values into the equation (2), the absolute value of d_{33} was calculated to be 72 pC/N. The reason for the high value of d_{33} estimated could possibly be due to an overestimation of Q/A from the device analysis. Capacitive coupling of bottom gate dielectric (PVCN) layer to the CYTOP dielectric of the dual-gate OFET led to a reduced V_{th} shift, hence leading to a high Q/A estimated as charges produced by the P(VDF-TrFE) sensing layer. Therefore, more studies using P(VDF-TrFE) as top-gate dielectric for the dual-gate OFET may give accurate d_{33} values estimated.

5.3. Summary and Conclusion

In this chapter, the dual-gate organic pressure sensor operation mechanism was investigated by estimating d_{33} of the P(VDF-TrFE) sensing layer to be 72 pC/N. This value reasonably agrees with d_{33} of the P(VDF-TrFE) films directly measured. Furthermore, a sensing voltage lead to V_{th} shift when pressure was exerted on the film; this was due to the piezoelectric behavior of the film. The V_{th} was typical of a dual-gate OFET with a top-gate OFET equivalent to the sensing voltage produced by the P(VDF-TrFE) film. This gave rise to the conclusion that the device is a dual-gate OFET based organic pressure sensor with polarized P(VDF-TrFE) sensing voltage and low-voltage bottom-gate OFET when a pressure load is placed on it. These results could be of interest for the development of organic pressure sensors using dual-gates, with one gate producing sensing voltage in response to pressure load and the other gate controlling the OFET operation.

References

[1] S. Iba, T. Sekitani, Y. Kato, T. Someya, H. Kawaguchi, M. Takamiya, T. Sakurai, S. Takagi, Appl. Phys. Lett. **87** (2005) 023509.

[2] M.-J. Spijkman, K. Myny, E. C. P. Smits, P. Heremans, P. W. M. Blom, D. M. de Leeuw, Adv. Mater. **23** (2011) 3231-3242.

[3] F. Maita, L. Maiolo, A. Minotti, A. Pecora, D. Ricci, G. Metta, G. Scandurra, G. Giusi, C. Ciofi, and G. Fortunato. IEEE Sensors Journal. **15** (2015) 3819-3826

[4] S. Hannah, A. Davidson, I. Glesk, D. Uttamchandani, R. Dahiya, H. Gleskova. Organic Electronics **56** (2018) 170-177

[5] R.S. Dahiya, G. Metta, M. Valle, A. Adami, and L. Lorenzelli. Applied Physics Letters, **95** (2009) 034105

[6] Y. Tsuji, H. Sakai, L. Feng, X. Guo and H. Murata. Applied Physics Express **10** (2017) 021601

[7] R.S. Dahiya, G. Metta, M. Valle, IEEE Trans. Ultrason., Ferroelectr., Freq. Control. **56** (2009) 2

[8] ANSI/IEEE, IEEE standard on piezoelectricity. IEEE Standard 176-1987 (1987)

[9] F. Maddalena, M. Spijkman, J. J. Brondijk, P. Fonteijn, F. Brouwer, J. C. Hummelen, D. M. de Leeuw, P. W. M. Blom, B. de Boer, Org. Electron. **9** (2008) 839-846

[10] X. Zhang, J. Hillenbrand and G.M. Sessler. Applied Physics Letters, 101 (2007) 054114

[11] K. S. Ramadan, D. Sameoto, and S. Envoy. Smart Mater. Struct, 23 (2014) 033001

[12] K. Takashima, S. Horie, M. Takenaka, T. Mukai, K. Ishida and Y. Ueda. J. Solid Mech. Mater. Eng. 6 (2012) 975-988

CHAPTER 6: Polarized P(VDF-TrFE) surface potential investigation

In this chapter, the threshold voltage shift caused by surface charges on a polarized P(VDF-TrFE) film is quantitatively analyzed. The polarized P(VDF-TrFE) film was placed on the active layer of the OFET and a corresponding shift in transfer characteristics curve of the OFET was observed. The surface charge density on the polarized P(VDF-TrFE) layer was directly measured to be 1.42 nC/cm^2; while the surface charge density on the film was estimated to be 0.4 nC/cm^2 from results from a conventional dual-gate OFET.

6.1. Introduction

In chapter 3, dual-gate pressure sensor, using P(VDF-TrFE) as the sensing layer and a low-voltage OFET as amplifier was developed. When the electric field is passed through P(VDF-TrFE) film sandwiched between two parallel conductors, they could easily be polarized. This is due to the orientation of the dipole moments formed by the parallel C-F atom and C-H bonds leading to charges of equal and opposite magnitude on the surface of the film. Figure 6.1(a) and (b) shows the α and β phase of P(VDF-TrFE), respectively.

Figure 6.1. Chemical structure of (a) α-phase P(VDF-TrFE) (b) β-phase P(VDF-TrFE)

Hydrogen Carbon Fluorine

The β-phase orientation of the molecules induces these dipole moments. Due to their unique characteristics, they have been used for sensors, microgenerators and in microelectromechanical systems (MEMS) [1-6]. An initial shift in the transfer characteristics curve was observed when the polarized film was laminated on the active layer of the OFET [7]. This initial shift was due to the surface potential of the film when in contact with the active layer. The surface potential was induced by a poling voltage, which polarized the film, therefore, displacing the dipole moment per unit volume. The polarization of the film is proportional to the magnitude of the poling voltage or electric field. In addition, the polarization in the film is equal to the density of surface charges [8].

In chapter 3, only -1000 V of poling voltage was applied to polarize the film. In this chapter, the magnitude of the poling voltage was changed. The electrical output response of the polarized film

to different was recorded. A shift in the transfer characteristics curve is linear to the poling voltage. Thus, suggesting that the density of surface charges on the film is dependent on the magnitude of the poling voltage. The charges on the surface of the film were estimated using results from a conventional dual-gate OFET [9-11]. The values determined would be confirmed in future experiments from directly measuring the surface potential on the P(VDF-TrFE) film.

6.2. Experimental Methods

Glass substrates were cleaned in an ultrasonic bath using acetone for 5 min to remove organic contamination or residue. The glass substrates were further cleaned in semicol clean for 10 min. The glass substrates were rinsed in water for 5 min twice. Finally in IPA for 10 minutes. The substrates were dried using IPA vapor from boiling IPA at 240 °C for 3 min. Then further dried on a hot plate at 100 °C for 3 min. 30 nm Al gate electrodes were vacuum evaporated on the glass substrates. 210 nm PVCN dielectric film was formed by spin-coating 40 mg/ml concentration of PVCN in chlorobenzene. Residual chlorobenzene solvent in the film was evaporated by annealing the film on a hot plate for 1 h after crosslinking it by UV (λ = 254 nm) treatment for 2 h. Source/drain Ag electrodes (50 nm) where deposited by vacuum evaporation method with a shadow mask defining the channel length and width to be 50 μm and 2 mm, respectively. In order to form a good interface with the semiconducting layer, the Ag source, drain electrodes where immersed in pentafluorobenzenethiol solution (0.005 mol/L) for 2 min. The electrodes were exhaustively rinsed with ethanol, then dried briefly on a hot plate. Spin-coating 10 mg/ml of Polystyrene (M_w = 600,000, Sigma Aldrich) and TIPS-pentacene (Ossila) with 3:1 ratio at1000 rpm formed the semiconducting layer. Furthermore, the film form was annealed for 30 min at 100 °C (all in dry nitrogen). The thickness of the semiconducting layer was measured to be 70 nm.

To complete the dual-gate OFET fabrication process, a 950 nm-thick top gate dielectric layer was deposited by spin-coating CYTOP (CTL-809M) on the semiconducting layer at 2000 rpm. The film formed was dried by annealing on a hot plate for 20 min at 100 °C.

This was then followed with annealing for 30 min at 100 °C. Similar to blade-coating procedure in chapter 3, a metal-insulator-metal capacitor was fabricated by placing another atomically clean

si substrate on the P(VDF-TrFE) film. The film was formed by blade coating 3 times for 3 minutes duration intervals during which the substrate is placed on a hot plate at 140 °C. To further crystallize the film formed, it was annealed at 140 °C for 2 hrs. To polarize the film dc voltage was applied to polarize the P(VDF-TrFE) film at -250 V, -500 V, -750 V and -1000 V respectively. The film was laminated on the active layer of a bottom-gate OFET after each polarization condition and the electrical output changes recorded. Direct measurement of the surface potential induced by polarizing the P(VDF-TrFE) film done by using a Digital Low Static Meter (MODEL KSD-3000).

6.3. Basic Parameters of OFET

Figure 6.2(a) and (b) show the transfer and output characteristics of the dual-gate OFET when the top-gate voltage, V_{TG} is grounded. Figure 6.2(a) shows the transfer characteristics of the low-voltage OFET by the sweeping gate voltage, (V_G) from 1 V to – 5 V while keeping the drain voltage, (V_D) constant at -5 V. The field effect mobility can be calculated from the saturation regime when $V_D > V_G$. The mobility, μ was calculated from drain current in the saturation regime equation (1):

$$I_{Dsat} = \frac{WC_i}{2L}\mu(V_G - V_{th})^2, \ldots\ldots\ldots\ldots (1)$$

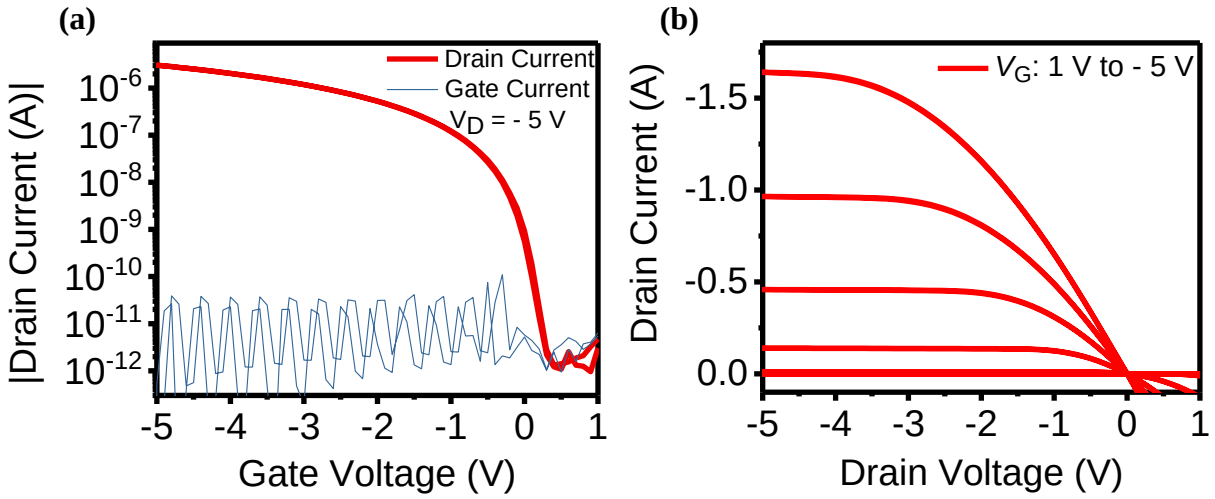

Figure 6.2. (a) Transfer and (b) output characteristics of the bottom-gate OFET

Where W and L are the width and length of the channel 2 mm and 50 μm respectively. C_i is the capacitance of PVCN, 13.4 nF/cm^2. ON/OFF ratio of the device is 2.32 ×10^6; μ is the mobility of the device in the saturation region, 0.46 cm^2/Vs; V_{th} was deduced to be -0.06 V from the intercept of $(I_D)^{0.5}$ against V_G; In addition, the subthreshold swing, (SS), 117 mV/decade was deduced from the equation below (2):

$$SS = \frac{\partial \log I_D}{\partial V_G}, \quad \ldots\ldots\ldots\ldots (2)$$

For the output characteristics (see Fig. 6.2(b)), the drain current I_D was measured while V_D varied with a constant V_G. As seen in Figure 6.2(a) the low-voltage OFET exhibited typical p-type characteristics with a linear increase in I_D with at low V_D, as well as saturation region with the increase in V_D.

6.4. Surface potential Discussion

When the polarized P(VDF-TrFE) was placed on the active layer of the OFET (TIPS-pentacene), the shift in threshold voltage was observed; this shift depends on the magnitude of the poling voltage. The surface potential generated by charges on the surface of the P(VDF-TrFE) layer with poling voltage of -250 V lead to V_{th} shift from 0.025 V to -0.005 as seen in Fig. 6.3(a). On increasing the magnitude of the poling voltage to -500 V, V_{th} shift was observed to have increased to -0.02 V. No V_{th} change was observed when the poling voltage was increased from

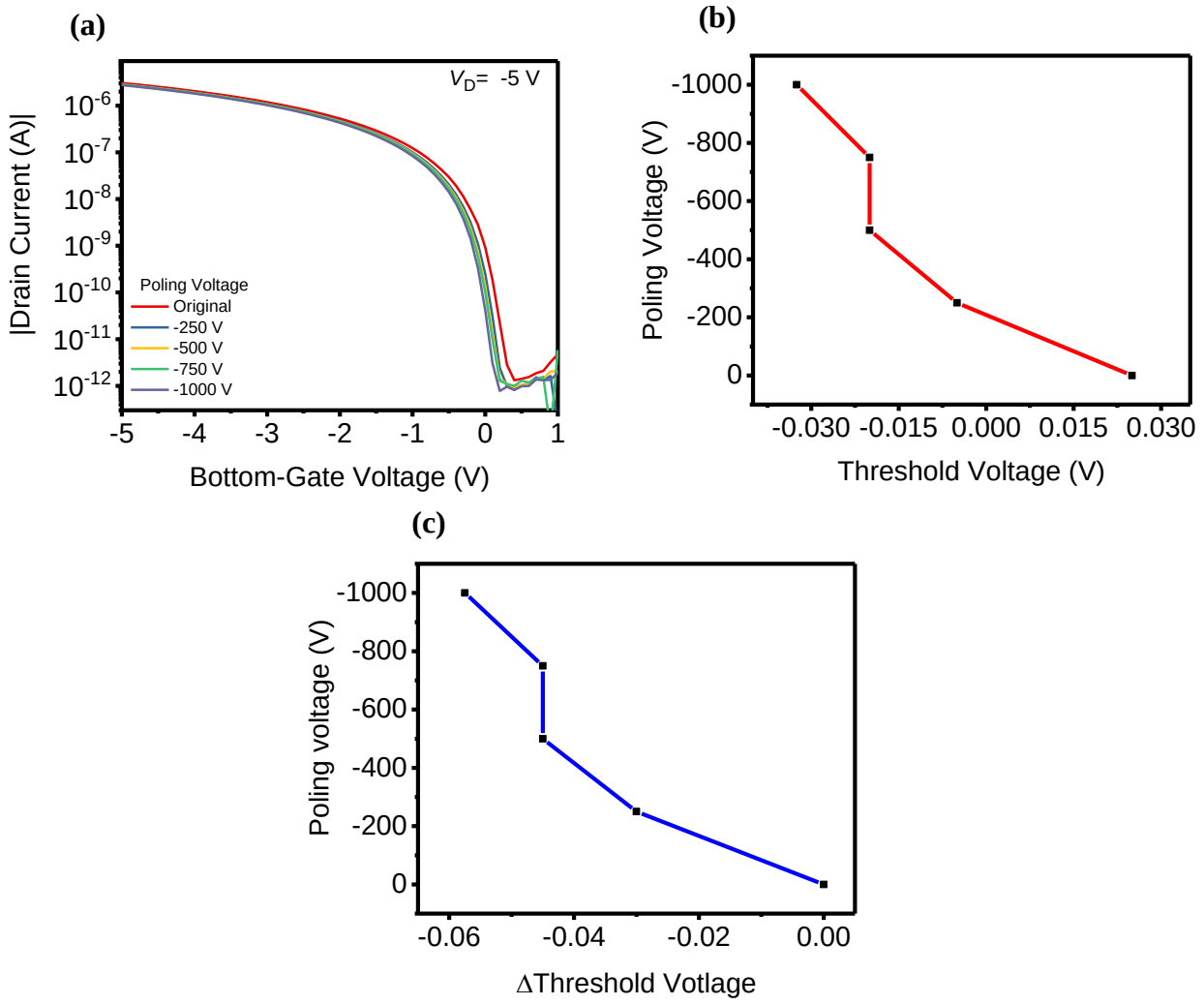

Figure 6.3(a) Transfer characteristics curve in response to different magnitude of poling (b) graph of poling voltage against threshold voltage (c) graph of poling voltage against change in threshold voltage.

-500 V to -750 V. This may be due to the incomplete polarization of the piezoelectric film, since the magnitude of electric field strength required to polarize the P(VDF-TrFE) film adequately is 80-100 V/μm [11]. Figure 6.3 (b) shows the relation between the threshold voltage and the poling voltage while Fig. 6.3 (c) shows the graph of poling voltage against threshold voltage shift with the initial threshold voltage value taken to be zero.

The β-form crystal orientation of the film strongly depends on the magnitude of the poling voltage. Excessive poling of the P(VDF-TrFE) film may have created trapping sites for charges injected into the film due to continuous application of electric field to polarize the film [12]. Increasing the poling voltage may have increased the β-form content of the material, hence the degree of polarization exhibited by the material. The surface potential created at the interface of the piezoelectric layer and the semiconducting layer may be due to charges injected into the film by continuous poling coupled with the β-form induced surface charges that screened the mobile charge carriers in the semiconducting channel of the OFET, hence, the shift in transfer curve observed in Figure 6.3(a).

The top-gate voltage/surface potential generated by the polarized P(VDF-TrFE) film can be estimated from the surface charges per unit area, *Q/A* using equation (3):

$$Q/A = \varepsilon_{P(VDF-TrFE)} V/d \quad \ldots\ldots\ldots \quad (3)$$

Where *V* and *d* (12 μm) is the surface potential and thickness of the polarized P(VDF-TrFE) film respectively; and $\varepsilon_{P(VDF-TrFE)}$ is the permittivity of P(VDF-TrFE). The surface potential was measured to be an average value of -213.7 V when the film was polarized with a poling voltage of -1000 V. Given the capacitance of the P(VDF-TrFE) film to be 6.741E-12 Farad, and substituting the permittivity of P(VDF-TrFE) into equation (3) the surface charge density on the piezoelectric

film was calculated to be 1.42 nC/cm^2. This is the surface charge density on the polarized film when measured directly.

In order to confirm the surface charge density measured directly, the quantity of surface charge per unit area (Q/A) generated by the polarized P(VDF-TrFE) film when placed on the OFET active layer can be estimated from results of a conventional dual-gate OFET [13,14] using equation (4):

$$Q/A = C_T V_{Top} \text{ …..…..…..} \quad (4)$$

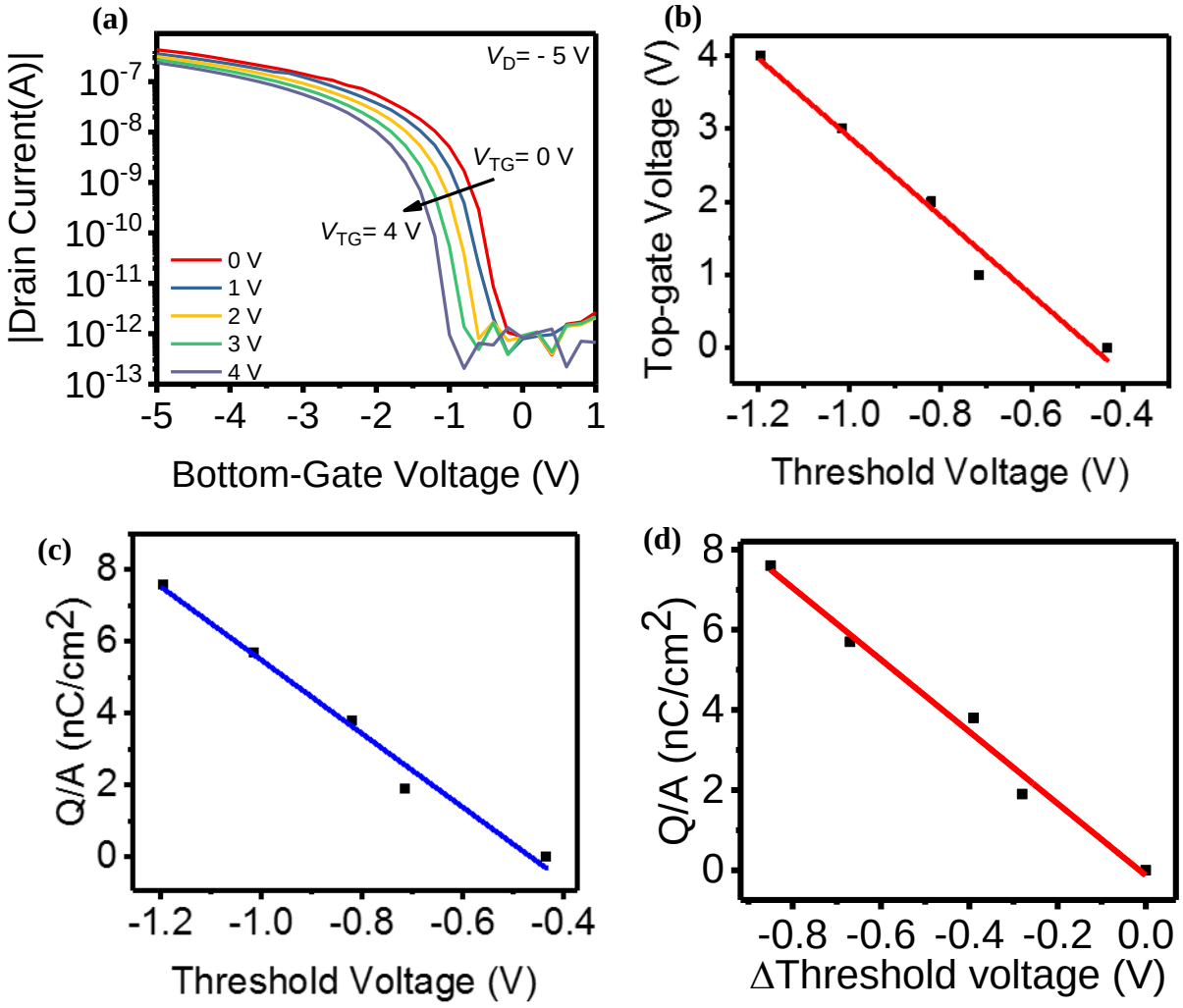

Fig. 6.4. Graph of (a) V_{th} shift of the OFET corresponding to V_{TG} (b) V_{TG} against V_{th} (c) charge per unit area against V_{th} (d) charge per unit area against change in V_{th}.

Where C_T (1.9 nF/cm^2) is the capacitance per unit area of Cytop. Figure 6.4 (a) shows shift in the transfer characteristics curve with increasing top gate voltage. V_{th} increased from -0.435 V to -1.195 V when V_{TG} was applied from 1 V to 4 V in step 1 V. A graph of the top-gate voltage against V_{th} shows a linear relation (see Fig. 6.4(b)). Using equation 4, the number of charges on the piezoelectric film was estimated. A linear relation between the surface charges per unit area to V_{th} is shown in Fig 6.4(c). Using this information, the surface charge density per unit V_{th} is determined from the slope of the graph to be -10 nC/cm^2 per V. Taking initial V_{th} to be zero, the graph of surface charge density against change in V_{th} is shown in Fig. 6.4 (d). Therefore, to extrapolate the surface charge density on the piezoelectric layer, V_{th} shift induced by the poling voltage is matched with equal value of V_{th} shift from the dual-gate OFET result shown in Fig. 6.4(d). In Fig. 6.3(c), using a -1000 V poling voltage, the V_{th} shift observed is -0.0575 V. The estimated surface charge density was extrapolated from Fig. 6.4(d) to be approximately 0.4 nC/cm^2. The estimated surface charge density on the polarized film is 72 percent lower than the surface charge density measured directly from the polarized film; thus, this experiment has to be repeated so as to give a more holistic comparison of the surface charge density estimated to that directly measured.

6.5. Conclusion

In summary, the surface charges density on a polarized P(VDF-TrFE) film induced by an electric field at different magnitude was investigated. A relation between the poling voltage and corresponding V_{th} shift was obtained. Using results from a dual-gate OFET, the surface charge density per unit V_{th} on the polarized P(VDF-TrFE) film when laminated to the semiconducting layer was estimated to be 72 percent lower than the surface charge density measured directly. Therefore, further investigation is required to explain differences in the results obtained.

References

[1] S. Dahiya, G. Metta, M. Valle, A. Adami, and L. Lorenzelli. Applied Physics Letters, **95** (2009) 034105

[2] F. Maita, L. Maiolo, A. Minotti, A. Pecora, D. Ricci, G. Metta, G. Scandurra, G. Giusi, C. Ciofi, and G. Fortunato. IEEE Sensors Journal. **15** (2015) 3819-3826

[3] S. Hannah, A. Davidson, I. Glesk, D. Uttamchandani, R. Dahiya, H. Gleskova., Organic Electron **56** (2018) 170-177

[4] K. Takashima, S. Horie, T. Mukai, K. Ishida, & K. Matsusshige. Journal of Robotics Society of Japan. **26** (2008) 711-717.

[5] Z. Pi, J. Zhang, C. Wen, Z-B. Zhang, D. Wu. Adv. Mater. **7** (2014) 33-41

[6] P-H Ducrot, I. Dufour, C. Ayela., Sci. Rep., **6** (2016) 19426

[7] Y. Tsuji, H. Sakai, L. Feng, X. Guo and H. Murata. Applied Physics Express **10** (2017) 021601

[8] M.A. Gottlieb, R. Pfeiffer 2013, California Institute of Science and Technology, accessed 9 May 2019 <http://www.feynmanlectures.caltech.edu/II_10.html>

[9] S. Iba, T. Sekitani, Y. Kato, T. Someya, H. Kawaguchi, M. Takamiya, T. Sakurai, S. Takagi, Appl. Phys. Lett. **87** (2005) 023509.

[10] M.-J. Spijkman, J. J. Brondijk, T. C. T. Geuns, E. C. P. Smits, T. Cramer, F. Zerbetto, P. Stoliar, F. Biscarini, P. W. M. Blom, D. M. de Leeuw, Adv. Funct. Mater, **20** (2010) 898- 905.

[11] P-H. Ducrot, I. Dufour, C. Ayela, Sci. Rep., **6** (2016) 19426.

[12] N. Murayama, T. Oikawa, T. Katto, K. Nakamura., J. Polym. Sci. B., **13** (1975) 1033-1047

[13] M.-J. Spijkman, K. Myny, E. C. P. Smits, P. Heremans, P. W. M. Blom, D. M. de Leeuw, Adv. Mater. **23** (2011) 3231-3242.

[14] O.O. Ogunleye, H. Sakai, Y. Ishii, H. Murata., Org. Electron., **75** (2019).

CHAPTER 7 || CONCLUSION AND FUTURE WORK

7.1. Conclusions

Studies on the sensing mechanism of a dual-gate pressure sensor based on P(VDF-TrFE) as sensing film and a low-voltage OFET as amplifier was thoroughly researched on. The piezoelectric constant, d_{33} of the film was estimated to be 72 pC/N. This value agrees with directly measured d_{33}, 53 pC/N of the film using a piezoelectric measurement system. In addition, the magnitude of surface potential to the degree of polarization was partly investigated. However, before getting to this final point of the research, some results had to be achieved as summarized below:

Chapter 1

A broad introduction of dual-gate pressure sensor was carried out. It started with the sensing regimes to transduction mechanism then further down to OFET based pressure-sensing devices. This chapter echoes the use of high operation voltage OFET for pressure sensing devices as well as the imperative for carrying out this research.

Chapter 2

In this chapter, low-voltage OFET devices were fabricated and characterized. First, using PVCN as dielectric, second, using a novel biopolyamide as the dielectric. Transfer and output characteristics were typical of a p-type OFET. While the PVCN layer required curing (UV crosslinking), the already synthesized biopolyamide did not require curing, therefore less time consuming during the OFET fabrication process.

Chapter 3

In this chapter, a dual-gate pressure sensor was fabricated. First, the read-out element was fabricated using reproducible experimental conditions in chapter 2, then the P(VDF-TrFE) film was formed by blade coating. The crystallized film was laminated on the active layer of the low-voltage OFET, and a shift in threshold voltage was observed. V_{th} was shown to be linear to the corresponding applied pressure.

Chapter 4

In this chapter, a 950 nm thick CYTOP was deposited on the active layer of the low-voltage OFET described in chapter 2. This formed the top-gate dielectric of a dual-gate OFET; then 50 nm thick Al electrode was vacuum evaporated on the CYTOP film to complete the fabrication procedure of a dual-gate OFET. Applying top-gate voltage, the V_{th} could be controlled, such that the relationship between it and the top-gate voltage is linear.

Chapter 5

The sensing mechanism of the pressure sensor was confirmed by quantitatively determining the piezoelectric constant, d_{33} of the piezoelectric (PVDF-TrFE) film to be 72 pC/N. In addition, this value was confirmed by measuring d_{33} of the film directly to be 53 pC/N.

Chapter 6

The surface potential on the P(VDF-TrFE) film was partly investigated by changing the poling voltage condition. Increasing the poling voltage led to a corresponding increase in V_{th} shift indicating that the polarization of the film was equally increased. The surface charges per unit area required to cause a unit shift in V_{th} was also quantified.

7.1. Future Work

The dual-gate organic pressure sensor in this research measures pressure signals above or equal to 100 kPa; therefore, there is a need to reduce the pressure region in which these pressure sensors could function. Reducing the pressure region below 113 kPa means they could for electronic skin which is a relevant topic today because of the possible applications for health care and robotics

For the pressure sensor, the OFET device was fabricated on a glass substrate, while the sensing element P(VDF-TrFE) was on a Si substrate. Therefore, the pressure sensor has its drawback, which means it cannot be used for flexible devices. Using flexible substrates such as polyethylene naphthalate (PEN) and polyethylene terephthalate (PET) the flexible dual-gate organic pressure sensors could be fabricated.

For commercial use of these pressure sensors, a high-throughput production process is required. Hence, the pressure sensing devices could be printed once on large flexible substrates in a timely fashion.

LIST OF ACHIEVEMENTS

JOURNAL

1. Ogunleye Olamikunle Osinimu, Heisuke Sakai, Yuya Ishii, Hideyuki Murata. "Investigation of the sensing mechanism of dual-gate low-voltage organic transistor based pressure sensor**",** vol. 79, Organic Electronics (accepted)

2. Ogunleye Olamikunle Osinimu, *et al*. Biopolyamide as the gate dielectric for low-operation voltage solution-processed organic field-effect transistors. (Manuscript in preparation)

CONFERENCES

1. Ogunleye Olamikunle Osinimu, Yohei Yoshinaka, Heisuke Sakai, Tatsuo Kaneko, and Hideyuki Murata. "A Biodegradable Biopolymer as Dielectric for Low-Voltage Solution-Processed Organic Field-Effect Transistors", *International Symposium on Organic Electronic Molecular Electronics*, Saga, Japan. May 31st – June 2nd, 2018.

2. Ogunleye Olamikunle Osinimu, Heisuke Sakai, Yuya Ishii, Hideyuki Murata. "Investigation of the Sensing Mechanism of the Dual-gate Low-voltage Organic Transistor based Pressure Sensor", *International thin-film transistor conference*, Okinawa, Japan. Feb. 28th – Mar. 2nd, 2019.

3. Ogunleye Olamikunle Osinimu, Heisuke Sakai, Yuya Ishii, Hideyuki Murata. "Investigation of the Sensing Mechanism of the Dual-gate Low-voltage Organic Transistor for Pressure Sensing by Quantitative Analysis", *JSAP spring meeting*, Tokyo, Japan. Mar. 9th – Mar.12th, 2019.

GRANT

Principal investigator for JAIST Research Grant (Fundamental Research) 2018

Title of Research Project: Investigation of the sensing mechanism in dual-gate low voltage organic transistor based pressure sensors.